

# Quantum Chaos in Quantum Wells

E. E. Narimanov and A. Douglas Stone

*Applied Physics, Yale University, P.O. Box 208284, New Haven CT06520-8284*

(October 26, 2018)

## I. INTRODUCTION

Although the field of quantum chaos found its first experimental challenges in atomic physics, during the past eight years several systems in condensed matter physics have been identified and studied from this point of view. In all of these cases the low-temperature electronic conduction properties of semiconducting heterostructures have been measured and analyzed to infer properties of the electronic spectrum and wavefunctions which may reveal quantum manifestations of chaos, or of the transition to chaos. Of these experiments, those which have involved patterning of two-dimensional electron gas systems to create more complex geometric scattering have in general not been amenable to detailed semiclassical analysis because the precise nature of the underlying confinement potential is not known. In contrast, the series of experiments performed at Nottingham University<sup>1</sup> and Bell Laboratories<sup>2</sup> which we will review and analyze here, involve tunneling through a quantum well in high magnetic field, for which the classical dynamics within the well can be accurately modelled and related to experimental observables. Moreover this system is unique in that three *in situ* experimental parameters, magnetic field,  $B$ , bias voltage  $V$ , and the angle between the electric and magnetic field,  $\theta$  can be continuously varied so as to generate a transition from integrable to (essentially) fully chaotic dynamics. As such the system provides an ideal testing ground for semiclassical methods; we will find that it also raises some new questions in non-linear dynamics of some general theoretical interest. We will review and summarize below our theoretical study of this system<sup>3-5</sup>, while also extending our earlier semiclassical treatment of the problem<sup>5</sup>.

We begin with some essential background. It is possible to fabricate atomically-flat layered materials, typically of the semiconductor GaAs and the insulator AlGaAs, such that the band-gap varies in a controlled manner along the longitudinal (growth) direction. This creates an effective one-dimensional potential for the electrons along this direction which confines the free electrons or holes (which are introduced by doping) in the semiconducting layers, known as “quantum wells”. In the experiments in question, a thin “emitter” layer is fabricated with only one longitudinal quantum level filled by doping, followed by a barrier, a wide ( $\sim 120$  nm) empty quantum well, a second barrier, and a conducting “collector” region. Thus one has in the longitudinal direction the potential profile of a “resonant tunneling diode”. As the voltage across the wide well is varied, states in the well can become aligned with the emitter level, and resonances in the tunneling current through the double-barrier structure will be measured if emitter and well states are coupled. In the experiments we will discuss, a large magnetic field is imposed, initially perpendicular to the layers, and has the effect of quantizing the electronic states within the layers into highly degenerate Landau levels. The electronic density in the emitter is such that typically only the lowest ( $n=0$ ) Landau level is full, and so an exact selection rule forbids tunneling through any but the  $n=0$  states of the well. Since both the emitter and well states have the same linear energy variation with  $B$ , one measures a series of peaks in the I-V characteristic of the device with voltage spacing corresponding to the longitudinal quantum states of the well, independent of the value of the magnetic field. Resonant tunneling diodes (RTDs) of this type have been well-studied for more than a decade.

The novel features of the more recent experiments arose when the magnetic field was tilted with respect to the electric field (tunneling) direction. We choose coordinates such that the normal direction to the layers is the  $z$ -direction, and the tilt angle is in the  $y$ - $z$  plane, so that  $\mathbf{B} = \cos\theta\hat{z} + \sin\theta\hat{y}$  (see Fig. 1). It was observed by Fromhold et al.<sup>1</sup> that as the tilt angle was varied at high magnetic field ( $B=10$ T), the frequency of resonance peaks in the I-V would abruptly change at certain values of the voltage (typically this frequency approximately doubled). These workers initially attributed this frequency-doubling to a density of states (DOS) effect within the well. They showed numerically that at large tilt angles the electron dynamics in the well is almost completely chaotic, and that there exist new unstable periodic orbits which collide with both the emitter and collector barriers. These orbits were supposed to give rise (at certain voltages) to additional DOS oscillations via Gutzwiller’s Trace Formula. A later numerical analysis of the quantum states within the well found that, unlike the usual level-clustering expected from the Trace Formula, in this case individual levels were scarred by the relevant periodic orbits once within each period of the Gutzwiller oscillation. Moreover, upon solving for the tunneling current by a quantum transfer matrix method it was found that in many cases these scarred levels carried essentially all of the resonant tunneling current<sup>6,7</sup>.

Additional interesting features of this system were found when Muller et al.<sup>1</sup> at Bell Labs undertook a careful study of the entire parameter space of magnetic field ( $0 < B < 12$ T), voltage ( $0 < U < 1$ V) and tilt angle, focusing

particularly on the transition region to chaos. They analyzed this large data set by plotting the peak locations in the B-V plane for fixed tilt angles between eleven and forty-five degrees. This representation of the data revealed a regions of peak-doubling and tripling which evolved in a complex manner with increasing tilt angle. These experiments motivated Shepelyansky and Stone<sup>8</sup> to analyze the global phase-space structure of electron motion within the well. Using a simplified model which neglected collisions with the emitter barrier they were able to estimate via the Chirikov resonance overlap criterion<sup>9</sup> the transition to global chaos in this system as a function of B,V, $\theta$ . They also suggested that the onset of peak-doubling in the system was due to bifurcations of the simplest “traversing orbit”, an interpretation adopted and amplified upon by Muller et al.<sup>2</sup>. However the classical analysis of Shepelyansky and Stone was not suitable for a developing a quantitative semi-classical theory, since it did not describe orbits which collide with both barriers, which dominate the tunneling spectrum according to both semiclassical theory<sup>5</sup> and exact quantum analyses<sup>6,7,10,11</sup>.

The initial experimental and theoretical/numerical results on this system raised a number of very interesting questions:

1) Is it possible to formulate a semiclassical theory of the tunneling current which involves only real (as opposed to complex) orbits within the well? If so, would such a theory only involve periodic orbits (and not all closed orbits as one finds in diamagnetic hydrogen), and would all or only a subset of the periodic orbits be important?

2) The classical dynamics of electron motion within the well was observed numerically to have some unusual features. Certain regions of phase space became highly chaotic well before a KAM analysis would predict. Moreover, periodic orbits which connected the emitter and collector barriers were observed to disappear by backwards bifurcations, but it was rarely if ever possible to find the bifurcations in which these orbits were born. What was causing these unusual properties?

3) Was the scarring of chaotic wavefunctions unusually common in this system? If so, what was the origin of this strong scarring, and why were only certain unstable periodic orbits reflected in the observed scarred wavefunctions?

We attempt to give answers to all of these questions below, based on analysis of the classical dynamics and semi-classical methods. We note that this system has been extensively studied numerically, both classically via the Surface-of-Section method<sup>8,3,12</sup>, and quantum-mechanically by analysis of scaled spectra<sup>10,11</sup> and tunneling current<sup>6,7,10,11</sup>. In addition to our own semiclassical treatment of the problem<sup>5</sup>, recently there has been an independent work by Bogomolny and Rouben which presents two possible semiclassical tunneling formulas for this system<sup>13</sup>. The first of these expressions neglects the structure of the emitter wavefunction and leads to a result which differs substantially from our periodic orbit formula, Eq. (18) below. In Ref.<sup>14</sup> the second was shown below to be equivalent to our Eq. (18), first presented in Ref.<sup>5</sup>, when similar assumptions were made about the emitter state (we present a similar proof and detailed comments below).

Recent comparisons of this formula with exact quantum calculations<sup>14</sup> and with experimental data<sup>5,14</sup> find good agreement. However, the periodic orbit formula was shown to lose accuracy and in some cases fail badly in narrow regions<sup>15</sup> near bifurcations, when the relevant periodic orbit does not yet exist or is not isolated. This failure is a manifestation of the “ghost” effect<sup>16</sup>. The relevance of this effect to the tilted well was first pointed out by Monteiro et al.<sup>10</sup> who have recently shown that an adequate semiclassical description in this regime can be achieved by using complex dynamics<sup>17</sup>. Alternatively, we show below that one can use a representation of the tunneling current in terms of closed orbits (Eq. 14, section IIB), which involves only real orbits within the well and provides a remarkably precise quantitative description of the ghost effect (see section IVB). It is important to note that for the tilt angles of interest the spectrum cannot be calculated perturbatively from the  $\theta = 0$  limit, so that the *only* analytic option is a semiclassical approach, exploiting the fact that we are interested in states far above the ground state of the well, and the large level-broadening as discussed below.

## II. SEMICLASSICAL THEORY OF RESONANT TUNNELING

### A. Bardeen Approximation

In standard tunneling theory the current will be proportional to the transmission coefficient from the emitter to the collector<sup>18</sup>. This presents an immediate complication for a semiclassical formulation of the problem because the transmission coefficient involves the Green function across classically forbidden regions and hence would involve complex paths traversing the barriers. However another aspect of the physics suggests an alternative and simpler approach. The electrons are injected by tunneling from the emitter state into the well under high bias and far from equilibrium. Hence they will emit optic phonons and lose energy over a time scale of 0.1ps corresponding to 4-5 collisions with the barriers, a time much shorter than the total tunneling time through the well which (from the measured tunneling current) corresponds to  $\sim 100 - 1000$  collisions. Therefore there is a substantial level-broadening,

corresponding to several level-spacings within the well, and the tunneling is sequential, not coherent. Under such circumstances, in which correlations between tunneling into and out of the well can be ignored, one may employ the Bardeen tunneling formalism<sup>19</sup>.

In Bardeen's "tunneling hamiltonian" approach, the system is treated as a sum of three isolated parts - the emitter, the quantum well, and the collector. Tunneling is considered as a perturbation, which introduces a nonzero coupling between these subsystems. The tunneling rate is then calculated using the Fermi Golden Rule, with the coupling matrix element expressed in terms of the wavefunctions of the isolated subsystems. One can then write a system of rate equations, expressing the balance of tunneling currents to and from the quantum well, and determine the nonlinear conductance of the system.

If the transmission coefficients of the emitter and collector barriers are of the same order of magnitude, a substantial space charge is accumulated in the quantum well. As a result, the electron-electron interactions in the well become relevant, and it is not possible to connect the properties of resonant tunneling spectra to the classical mechanics of a *single* electron in the well. In order to probe the single-electron dynamics in the quantum well, the charge build-up in the well must be prevented. That can be achieved only when the width of the collector barrier is much thinner than the width of the emitter barrier, so that the tunneling rate from the well to the collector is much larger than the tunneling rate from the emitter to the well. In such a case we may set the occupation number of states in the well to zero in the rate equations for the current.

In this regime the rate limiting step is the tunneling from the emitter to the well, and the tunneling current is therefore proportional to the corresponding *tunneling rate* (probability of tunneling per unit time). If there is only one energy level occupied in the emitter 2DEG (which is the case in the experiment at high magnetic fields  $B \geq 5\text{T}$ ), the tunneling current  $j$  is given by

$$j = n_e e W^{e \rightarrow w} \quad (1)$$

where  $n_e$  is the surface concentration in the emitter layer. The Eq. (1) can be easily generalized to the case, when the emitter layer contains several occupied single-electron levels.

The tunneling rate from the emitter to the well

$$W^{e \rightarrow w} = \frac{2\pi}{\hbar} \sum |M^{e \rightarrow w}|^2 \delta(\varepsilon_w - \varepsilon_e) \quad (2)$$

where the summation is performed over all energy levels in the well, and the coupling matrix element<sup>19,18</sup> is given by

$$M^{e \rightarrow w} = \frac{\hbar^2}{2m^*} \int_S (\Psi^w \nabla \Psi^e - \Psi^e \nabla \Psi^w) d\mathbf{S} \quad (3)$$

with the wavefunctions  $\Psi_e$  and  $\Psi_w$  corresponding respectively to *isolated* emitter and *isolated* well.

The integration in (3) can be performed over any surface inside the barrier, including the boundary of the barrier itself. We choose to perform the integration over the "inner" boundary, which is classically accessible to the electrons trapped inside the well. The latter allows the semiclassical treatment of the wavefunctions of the isolated well using the Gutzwiller path integral approach<sup>20</sup>.

The expression (3) involves both the wavefunction of the isolated well  $\Psi^w$  and its normal derivative  $\nabla \Psi^w$ , taken at the surface of the barrier ( $z = 0$ ). In the limit of large height of the emitter barrier  $U_0$  corresponding to the experimental setup<sup>21</sup> the normal derivative of the wavefunction does not depend on  $U_0$ , while for the wavefunction itself calculated at the plane of the barrier the dependence on  $U_0$  is crucial:  $\Psi^w(z = 0) \sim \exp(-\sqrt{U_0/\varepsilon_i})$ , where the "injection energy"  $\varepsilon_i$  is defined as the difference between the total energy  $\varepsilon$  and the potential drop across the well  $eV$ . Since both terms in Eq. (3) are of the same order of magnitude, Eq. (3) requires an adequate representation of both the well wavefunction and its normal derivative.

The standard semiclassical path-integral approach, which includes only real classical trajectories, does not distinguish between infinite and finite potential barriers, and cannot be used for the calculation of the exponentially small, but non-zero value of the wavefunction at the plane of the barrier. This makes it complicated to apply directly the Eq. (3) to the semiclassical description of the resonant tunneling. Instead, we first reduce the expression (3) to the form, which involves only the normal derivatives of the wavefunction of the isolated quantum well<sup>22</sup>. In the leading order in  $\hbar\omega_c/U_0$ ,  $\varepsilon_i/U_0$  and  $eEa_e/U_0$  (where  $a_e$  is the width of the emitter barrier), the matrix element (3) can be expressed as

$$M_{nk}^{e \rightarrow w} = \frac{\hbar^2}{m^*} \int_{-\infty}^{\infty} dx \int_{-\infty}^{\infty} dy \Psi_n^e(x, y, 0) \left. \frac{\partial \Psi_k^w(x, y, z)^*}{\partial z} \right|_{z=0} \quad (4)$$

To obtain Eq. (4) we neglect the effects of the electric field and the transverse component of the magnetic field in comparison with  $U_0$  in barrier region  $-a_e < z < 0$ . Note, that for the untilted system ( $\theta = 0$ ) the approximation (4) gives *exactly* the same result as the standard WKB method.

With the choice of the vector potential  $\mathbf{A} = (-By \cos(\theta) + Bz \sin(\theta))\hat{\mathbf{x}}$  the system possesses translational symmetry in the  $x$ -direction. Therefore, the dynamics within the well can be reduced to two degrees of freedom (see below)  $y, z$ ,<sup>2,8,10,3</sup> with an effective potential  $V(y, z)$ . The well wavefunctions in Eq. (4) can be re-expressed in terms of the Green function of the isolated well,  $G(y_1, z_1 = 0; y_2, z_2 = 0; \varepsilon)$ :

$$W^{e \rightarrow w} = -\frac{2\hbar^3}{m^*{}^2} \Im \int \int dy_1 dy_2 \Psi_n^e(y_1, 0) \Psi_n^e(y_2, 0)^* \left. \frac{\partial^2 G(y_1, z_1; y_2, z_2; \varepsilon_n)}{\partial z_1 \partial z_2} \right|_{z_1=z_2=0} \quad (5)$$

The emitter state  $\Psi_e$  in Eq. (4) involves only the few lowest single-particle levels and can be calculated accurately using a variational approach<sup>23</sup>. The “injection function”  $\Psi_e(y, 0)$  is then a linear combination of the lowest few Landau level wavefunctions  $\Phi_n$ , and is peaked at an injection point  $y_i \approx (a_e + 1.13(\hbar^2/m^*eE)^{1/3}) \tan \theta$ , and has spatial extent of order the magnetic length,  $l_B \equiv \sqrt{\hbar/eB \cos \theta} \sim \hbar^{1/2}$ :

$$\Psi_e(y, 0) = l_B^{-1/2} \sum_n c_n \Phi_n \left( \frac{y - y_i}{l_B} \right) \quad (6)$$

## B. Semiclassical Approximation: The Closed Orbit Formula

In the semiclassical approximation<sup>20</sup>, the derivative of Green function  $\partial_{z_1 z_2}^2 G(y_1, z_1 = 0; y_2, z_2 = 0; \varepsilon)$  is determined by *all* classical trajectories connecting the points  $(y_1, 0); (y_2, 0) \equiv (y - \Delta y/2, 0); (y + \Delta y/2, 0)$ , and, as shown in Appendix A, can be expressed as:

$$\left. \frac{\partial^2 G(y_1, z_1; y_2, z_2; \varepsilon_n)}{\partial z_1 \partial z_2} \right|_{z_1=z_2=0} = \frac{8\pi}{(2\pi i)^{3/2} \hbar^{7/2}} \sum_\gamma (p_i^\gamma)_z (p_f^\gamma)_z D_\gamma^{1/2} \exp \left[ i \frac{S_\gamma(y - \Delta y/2, 0; y + \Delta y/2, 0; \varepsilon)}{\hbar} \right] \quad (7)$$

where  $S_\gamma(y - \Delta y/2, 0; y + \Delta y/2, 0; \varepsilon) \equiv S_\gamma$  is the action of the classical trajectory<sup>24</sup> indexed by  $\gamma$ ,  $D_\gamma$  is the appropriate amplitude<sup>20</sup>, and  $p_i^\gamma$  and  $p_f^\gamma$  correspond to the initial and final momenta of the trajectory. Substituting (7) into (5), and introducing the effective broadening  $\hbar/\tau_{\text{opt}}$  of the energy levels in the well, for the oscillatory part of  $W_{e \rightarrow w}$  we obtain:

$$W_{\text{osc}} = \int dp_y \int dy f_W(y, p_y) \sum_\gamma \frac{(p_i^\gamma)_z (p_f^\gamma)_z}{(m^*)^2} \int d\Delta y \Re \left\{ \frac{8D_\gamma^{1/2}}{\sqrt{2\pi\hbar i}} \exp \left[ -\frac{t_\gamma}{\tau_{\text{opt}}} + i \frac{S_\gamma - p_y \Delta y}{\hbar} \right] \right\} \quad (8)$$

where  $t_\gamma$  is the classical propagation time of the trajectory  $\gamma$ , and the factor  $\exp(-t_\gamma/\tau_{\text{opt}})$  represents the effect of phonon emission. This factor suppresses the coherent contributions of trajectories longer than  $\tau_{\text{opt}}$ .

We have also introduced in Eq. (8) the Wigner transform  $f_W^e$  of the emitter wavefunction

$$f_W^e(y, p_y) \equiv h^{-1} \int d\Delta y \Psi_e(y - \Delta y/2, 0) \Psi_e^*(y + \Delta y/2, 0) \exp(ip_y \Delta y/\hbar) \quad (9)$$

which describes the distribution in transverse position and momentum of electrons injected into the well. Since  $\Psi_e(y)$  has a width  $\sim l_B$ , the integrand in Eq. (8) will be small for  $\Delta y > l_B \sim \hbar^{1/2}$ .

Assuming that  $M$  Landau levels contribute to the emitter state wavefunction, then the Wigner function

$$f_W^e(y, p_y) = \frac{1}{\hbar l_B} \sum_{k', k''=0}^{M-1} \mathcal{U}_{k'k''} \left( \frac{y - y_i}{l_B} \right)^{k'} \left( \frac{p_y l_B}{\hbar} \right)^{k''} \exp \left\{ -\left( \frac{y - y_i}{l_B} \right)^2 - \left( \frac{p_y l_B}{\hbar} \right)^2 \right\} \quad (10)$$

where the coefficients  $\mathcal{U}_{k'k''}$  can be obtained from the relation

$$\sum_{k', k''=0}^{M-1} \mathcal{U}_{k'k''} \left( \frac{y - y_i}{l_B} \right)^{k'} \left( \frac{p_y l_B}{\hbar} \right)^{k''} \equiv \sum_{n', n''=0}^{M-1} c_{n'} c_{n''}^* I_{n'n''} \quad (11)$$

where

$$I_{n'n''} = (-1)^{\min(n', n'')} 2^{1+\frac{|n'-n''|}{2}} \frac{\min(n', n'')!}{\sqrt{n'! n''!}} \left( \frac{y-y_i}{l_B} - i \text{Sign}(n' - n'') \frac{p_y l_B}{\hbar} \right)^{|n'-n''|} \\ \times L_{\min(n', n'')}^{|n'-n''|} \left( 2 \left( \frac{y-y_i}{l_B} \right)^2 + 2 \left( \frac{p_y l_B}{\hbar} \right)^2 \right) \quad (12)$$

and  $L_n^m$  is the generalized Laguerre polynomial.

Consider first the integration over  $\Delta y$  in Eq. (8). Since  $\Delta y \sim \hbar^{1/2}$ , in the semiclassical limit  $\hbar \rightarrow 0$ , one can expand the scaled action  $S_\gamma(y - \Delta y/2, 0; y + \Delta y/2, 0; \varepsilon)/\hbar$  in  $\Delta y$ , retaining only terms up to second order, and perform exactly the resulting Gaussian integral. Alternatively, we can employ the approach of Berry<sup>25</sup> and perform this integration by stationary phase, which will initially lead to an expression in terms of non-closed orbits which satisfy the ‘‘mid-point rule’’, and then re-express this answer to the same accuracy in  $\hbar$  using  $\Delta y \sim \sqrt{\hbar}$  to arrive at the same result involving only families of closed orbits:

$$W_{\text{osc}} = \frac{16}{m^*} \int dy \int dp_y f_W(y, p_y) \sum_\alpha \sqrt{\frac{(p_i^\alpha)_z (p_f^\alpha)_z}{m_{11}^\alpha + m_{22}^\alpha + 2}} \exp \left[ -\frac{i}{\hbar} \frac{2m_{12}^\alpha}{m_{11}^\alpha + m_{22}^\alpha + 2} (p_y - \bar{p}_y^\alpha)^2 \right] \exp \left[ i \frac{S_\alpha(y, 0; y, 0; \varepsilon)}{\hbar} \right] \quad (13)$$

where  $M_\alpha \equiv (m_{ij}^\alpha)$  is the  $2 \times 2$  monodromy matrix<sup>20</sup>, defined via the linearization of the Poincaré map near the closed orbit  $\alpha$ , and calculated at the contact point at the emitter barrier.

The  $y$ -integration now involves the rapidly-varying phase  $\exp[iS_\alpha(y, y)/\hbar]$  for closed orbits beginning and ending at  $y$ . This phase is stationary for the periodic orbits, and we therefore expect the periodic orbits to determine the tunneling current. However,  $f_W(y)$  varies on the same spatial scale  $\sim \hbar^{1/2}$ , and we therefore cannot immediately perform the  $y$  integral by stationary phase (as is done to derive the trace formula for the total density of states<sup>20</sup>). The failure of such an approach in this case reflects a more general principle of semiclassical theory; experimental observables typically do not depend only on the density of states, but also upon coupling matrix elements. The classical orbits which will contribute then depend on the nature and spatial extent of the coupling. In fact in the well-known problem of diamagnetic hydrogen, the ‘‘source function’’ analogous to  $f_W(y)$  varies on a scale much smaller than the relevant phase, being effectively a delta-function, and the resulting semiclassical theory involves *all* closed orbits at the source point<sup>26</sup> and not periodic orbits. The current situation is intermediate between the absorption spectrum for diamagnetic hydrogen and a pure density of states measurement; a periodic orbit sum can describe the tunneling spectrum quantitatively, but a closed orbit formula (Eq. (14) below) is more accurate near bifurcations. However the periodic orbit formula cannot be obtained by stationary phase integration at this point<sup>27</sup>.

Since the emitter state Wigner function  $f_W^e$  has the spatial extent of the order of the magnetic length  $l_B \sim \sqrt{\hbar}$ , and exponentially decays away from this interval, one can expand the scaled action  $S/\hbar$  in the powers of the deviation  $(y - y_i) \sim \sqrt{\hbar}$  from the ‘‘injection’’ point  $y_i$  (defined as the center of  $f_W$ ) and keep only the terms up to the second order. The integration over  $y$  will then yield:

$$W_{\text{osc}} = \frac{8}{m^*} \Re \sum_\alpha \mathcal{A}_\alpha \sqrt{\frac{(p_i^\alpha)_z (p_f^\alpha)_z}{m_{11}^\alpha + m_{22}^\alpha + 2}} \exp \left\{ -\frac{t_\alpha}{\tau_{\text{opt}}} - \kappa_\alpha \left( \frac{\Delta p_y^\alpha l_B}{\hbar} \right)^2 \right\} \exp \left( i \frac{S_{\text{cl}}^\alpha}{\hbar} - i \frac{\pi n_\alpha}{2} \right) \quad (14)$$

where the summation is performed over closed orbits which start and end at the injection point  $y = y_i$ . Generically there will only be *one* such trajectory in each topologically distinct family of closed orbits and this orbit will *not* be periodic, i.e. there will be a non-zero difference between the initial and final momentum. In Eq. (14)  $S_{\text{cl}}^\alpha \equiv S_\alpha(y_i, 0; y_i, 0)$  is the action of this special closed orbit,  $n_\alpha$  is its topological index<sup>20</sup>, and  $\Delta p_\alpha$  is the difference between the ‘‘initial’’ and ‘‘final’’ momenta:  $\Delta p_y^\alpha = (p_f^\alpha)_y - (p_i^\alpha)_y$ . In (14) we have also introduced the following parameters:

$$\kappa_\alpha = \frac{1}{4(1 + \eta_\alpha^2)}, \quad \eta_\alpha = \frac{2 - \text{Tr}[M_\alpha] l_B^2}{2m_{12}^\alpha \hbar}, \quad \mathcal{A}_\alpha = \sum_{k' k''} \mathcal{U}_{k' k''} \mathcal{L}_{k' k''}^\alpha,$$

where the coefficients  $\mathcal{U}_{k' k''}$ , defined in (10), represent the ‘‘transverse’’ dependence of the emitter state wavefunction, and are non-vanishing only for the few lowest Landau levels ( $k', k'' \sim 1$ ). The general expression for the matrix element  $\mathcal{L}_{k' k''}$  is very complicated and will not given here. Here we only present the result for the most relevant<sup>1,3,10</sup> families of the closed orbits, for which  $\bar{p}_y^\alpha \equiv 0$ :

$$\mathcal{L}_{k' k''} = \left( \frac{i}{2} \right)^{k'+k''} (1 + i\eta_\alpha)^{-\frac{k'+1}{2}} \left( 1 + i \frac{\xi_\alpha}{\eta_\alpha} \right)^{-\frac{k''+1}{2}} H_{k'} \left( \frac{\Delta p_y^\alpha l_B}{2\sqrt{1 + i\eta_\alpha}} \right) \exp \left( -i\kappa_\alpha \eta_\alpha \left( \frac{\Delta p_y^\alpha l_B}{\hbar} \right)^2 \right) \quad (15)$$

where  $H_k(x)$  is the Hermite polynomial, and  $\xi_\alpha = (2 - \text{Tr}[M_\alpha]) / (2 + \text{Tr}[M_\alpha])$ .

As noted above, typically there is only one trajectory which reaches  $y_i$  out of each family of closed orbits and hence only one per family contributes to the tunneling rate in Eq. (14). Let us call this orbit the *injected orbit*. Although the number of injected orbits increases rapidly with the increase of the orbit length, the contributions of long orbits with the traversal time  $t_\alpha$  longer than the relaxation time  $\tau_{\text{opt}}$  are suppressed by the damping factor  $\exp(-t_\alpha/\tau_{\text{opt}})$ . Since  $\tau_{\text{opt}}$  generally corresponds to the time of a few traversals of the quantum well, it follows then that one may neglect all but the few shortest injected orbits and the sum in (14) is convenient for comparisons with experimental or numerical data.

It is worth emphasizing again that the trajectories which contribute to the Closed Orbit Formula (14) are typically not periodic. The Closed Orbit Formula (COF) is therefore free from the problems which are encountered in semiclassical periodic orbit sums near bifurcations when quadratic expansions fail. We present comparisons of this formula with exact numerical results below in Section IV.B, after outlining our theory of the classical mechanics in the tilted well. These comparisons indicate that the COF yields an excellent quantitative description of the ghost effect, which is important near bifurcations in this system<sup>16,10</sup>. The COF therefore represents a convenient alternative to the use of uniform approximations<sup>29</sup> and/or complex classical dynamics<sup>17</sup>. The Closed Orbit Formula, Eq. (14) is one of the main results of the current work.

### C. Periodic Orbit Formula

As follows from (14), only injected orbits with the difference between initial and final momenta  $\Delta p_y \sim \sqrt{\hbar}$ , can give substantial contributions to the tunneling current. Therefore for these important injected orbits, in the generic case (see Fig. 2) there exists one and only one periodic orbit (which has  $\Delta p_y = 0$ ) in a semiclassically small neighborhood near it. Using this proximity of each relevant injection orbit to a periodic orbit we can re-express the actions and momenta of the injection orbits in terms of the properties of their periodic neighbors (labeled by the index  $\mu$ ) as follows:

$$S_\alpha(y_i, 0; y_i, 0) \simeq S_\mu + \frac{\text{Tr}[M_\mu] - 2}{2m_{12}^\mu} (y_i - y_\mu)^2, \quad (16)$$

$$\bar{p}_y^\alpha \simeq p_y^\mu + \frac{m_{11}^\mu - m_{22}^\mu}{2m_{12}^\mu} (y_i - y_\mu) \quad (17)$$

and for the tunneling current we obtain

$$W_{\text{osc}} = \frac{16}{m^*} \int dy \int dp_y f_W^{(e)}(y, p_y) \sum_\mu \frac{p_z^\mu \exp\left(-\frac{T_\mu}{\tau_{\text{opt}}}\right)}{\sqrt{|m_{11}^\mu + m_{22}^\mu + 2|}} \cos\left[\frac{S_\mu}{\hbar} - \frac{\pi n_\mu}{2} + Q_\mu(\delta y, \delta p_y)\right] \quad (18)$$

where

$$Q_\mu = \frac{2 m_{21}^\mu (\delta y)^2 + (m_{22}^\mu - m_{11}^\mu) \delta y \delta p_y - m_{12}^\mu (\delta p_y)^2}{\hbar (m_{11}^\mu + m_{22}^\mu + 2)}.$$

Here  $\mu$  labels the periodic orbit,  $\delta y = y - y_\mu$ ,  $\delta p_y = p_y - (p_\mu)_y$ , the integer  $n_\mu$  is the topological index<sup>20</sup> of the periodic orbit, and the  $2 \times 2$  monodromy matrix<sup>20</sup>  $M = (m_{ij}^\mu)$  is calculated at contact point at the emitter barrier.

This relation between injected orbits and periodic orbits is generically valid because if  $\Delta p_y$  is small for the injected orbit, then the function  $\Delta p_y(y)$  for this family of closed orbits can be expanded linearly around  $y_i$  and extrapolated to zero to find the nearby periodic orbit (see Fig. 2(a)). However if that periodic orbit is in the neighborhood of a bifurcation this expansion will fail and Eq. (18) will become unreliable. The simple case of a tangent bifurcation is illustrated schematically in Fig. 2(b). Here just before the bifurcation there are two periodic orbits which are close together, neither of which alone can adequately describe the contribution of the relevant closed orbits. Just after the tangent bifurcation there is no periodic orbit at all in the semiclassically small neighborhood of the injected orbit. There may however be another periodic orbit of the same topology far away from the injected orbit - see Fig. 2(c). In this case the linear expansion will yield a semiclassically large value for  $\Delta p_y$  and it will not contribute to the sum, introducing no additional error, but missing higher-order contributions near the bifurcation. In such cases the periodic orbit formula (18) will lose accuracy but not fail completely as the resulting divergences are integrable (see Fig. 12 below). However for such cases the Closed Orbit Formula will remain quite precise and can be adapted for

the specific type of nearby bifurcation. In section IV.B we demonstrate this for the case of tangent bifurcations in which we calculate the exponentially small “ghost” contributions<sup>16</sup> beyond the bifurcation.

Eq. (18) has the feature that it separates out the semiclassical summation over periodic orbits within the well from the contribution of the injection function  $f_W^{(e)}(y, p_y)$  which cannot be calculated semiclassically and depends on the doping level in the emitter, as well as the magnetic field and tilt angle, thus it is convenient for a general quantitative description of the actual experiments. If the emitter state wavefunction has only zero-order Landau level component ( $\mathcal{L}_{k'k''} \sim \delta_{k'0} \delta_{k''0}$ ), then the integration in (18) can be performed analytically. For the most relevant periodic orbits with  $p_y = 0$  at the point of collision with the emitter barrier, we obtain:

$$W_{\text{osc}} = \frac{8\sqrt{2}}{m^*} \Re \sum_{\mu} \frac{p_z^{\mu} \exp\left(-\frac{T_{\mu}}{\tau_{\text{opt}}} - R_{\mu}\right)}{\sqrt{\text{Tr}[M_{\mu}] + 2i\left(\frac{m_{21}^{\mu}}{eB \cos\theta} - m_{12}^{\mu} eB \cos\theta\right)}} \exp\left[i\frac{S_{\mu} + \Delta S_{\mu}}{\hbar} - i\frac{\pi\tilde{n}_{\mu}}{2}\right] \quad (19)$$

where

$$\Delta S_{\mu} = \frac{\sigma_{\mu}}{1 + \sigma_{\mu}^2} eB \cos\theta (y_{\mu} - y_i)^2, \quad R_{\mu} = \sigma_{\mu} \Delta S_{\mu}, \quad \sigma_{\mu} = \frac{\text{Tr}[M_{\mu}] - 2}{2m_{12}^{\mu}} \frac{1}{eB \cos\theta}, \quad \tilde{n}_{\mu} = n_{\mu} + 1 - \text{Sign}(\text{Tr}[M_{\mu}] + 2).$$

If the shift of the “injection point”  $y_i$  from zero can be neglected, Eq. (19) reduces<sup>11</sup> to the result, obtained by Bogomolny and Rouben<sup>13</sup>.

The summation in (18) is performed over all isolated periodic orbits, both stable and unstable. Near stable islands the motion is regular and we expect semiclassical quantization to yield discrete energy levels (neglecting phonon broadening) and sequences of eigenfunctions localized on the islands<sup>30,10</sup>. In contrast near unstable orbits the motion is chaotic and semiclassical theory does not yield discrete levels<sup>20</sup>. This difference, can be displayed explicitly by performing exactly the summation over repetitions of the primitive periodic orbits in Eq. (18), yielding

$$W = \frac{8}{m} \sum_{\mu} (p_{\mu})_z \sum_{\ell} \Delta\left(\frac{T_{\mu}}{\tau_{\text{eff}}^{\mu}}, \frac{S_{\mu}(\varepsilon_{\ell})}{\hbar} - \frac{\pi n_{\mu}}{2}\right) \int dy \int dp_y f_W^e(y, p_y) g_{\ell}^{\mu, \pm}(y, p_y) \quad (20)$$

where  $\Delta(\sigma, \rho) = \frac{\sinh(\sigma)}{\cosh(\sigma) - \cos(\rho)}$ , and the index + or - denotes stable or unstable orbits. The quantity  $\hbar/\tau_{\text{eff}}^{\mu}$  is an effective level-broadening which differs in the two cases.

Note that the function  $\Delta$  has a peak every time the semiclassical quantization condition  $S_{\mu}(\varepsilon_{\ell}) = 2\pi\hbar(n + n_{\mu}/4)$  is satisfied, and these peaks become delta functions as  $\tau_{\text{eff}}^{\mu} \rightarrow \infty$ . For stable orbits we find that  $\tau_{\text{eff}}^{\mu} = \tau_{\text{opt}}$ , so if we neglect phonon scattering ( $\tau_{\text{opt}} \rightarrow \infty$ ) we do recover perfectly discrete contributions to the tunneling current. In the stable case the argument of  $S_{\mu}$  in Eq. (20) is  $\varepsilon_{\ell}^{\pm} \equiv \varepsilon - \hbar\omega_{\perp}^{\mu, \pm}(\ell + 1/2)$  which may be interpreted as the energy of longitudinal motion along the orbit. Due to the harmonic approximation the quantization of the transverse oscillations around the periodic orbit simply yields equally spaced levels<sup>10,30</sup> with spacing  $\hbar\omega_{\perp}^{\mu, \pm}$ , where the frequency  $\omega_{\perp} \equiv \phi_{\mu}/T_{\mu}$ ,  $\phi_{\mu}$  is the winding number<sup>20</sup> and  $T_{\mu}$  the period of the orbit. So the discrete energies at which tunneling occurs are the correct semiclassical energy levels of the well.

The amplitude of each contribution is given by the coefficient functions  $g_{\ell}$  in Eq. (20), which are the Wigner transforms of the harmonic oscillator wavefunctions corresponding to these transverse modes:

$$g_{\ell}^{\mu, +}(y, p_y) = (-1)^{\ell} L_{\ell} \left(2 \left|\tilde{Q}_{\mu}\right|\right) \exp\left(-\left|\tilde{Q}_{\mu}\right|\right) \quad (21)$$

where  $L_{\ell}$  is the Laguerre polynomial and  $\tilde{Q}_{\mu} = |2 + \text{Tr}[M]|^{1/2} |2 - \text{Tr}[M]|^{-1/2} Q_{\mu}$ .

Since the result (21) is based on the harmonic approximation within a stable island, we may only include modes up to  $\ell_{\text{max}}$ , which is given by the ratio of the island area to  $\hbar$ . Phonon scattering smears out each of these discrete contributions to  $W_{\text{osc}}$  over an energy range  $\hbar/\tau_{\text{opt}}$ .

In contrast, for unstable periodic orbits we find that  $\tau_{\text{eff}}^{\mu} = \tau_{\text{opt}}/(1 + \ell\lambda_{\mu}\tau_{\text{opt}})$ , where  $\lambda_{\mu}$  is the Lyapunov exponent near the orbit  $\mu$ . Hence this time is finite and equal to  $1/\lambda_{\mu}$  in the absence of phonon scattering. Therefore, instability acts as a sort of intrinsic level-broadening, and each PO describes a contribution due to a cluster of levels. The peak of the function  $\Delta$  in Eq. (20) corresponding to the mean energy of the cluster is given by  $S_{\mu}(\varepsilon) = 2\pi\hbar(n + n_{\mu}/4)$ . The weight functions

$$g_{\ell}^{\mu, -}(y, p_y) = (-1)^{\ell} \Re \left\{ L_{\ell} \left(2i\tilde{Q}_{\mu}\right) \exp\left(i\tilde{Q}_{\mu}\right) \left(1 + i\frac{\sin(S_{\mu}/\hbar - \pi n_{\mu}/2)}{\sinh(T_{\mu}/\tau_{\text{eff}}^{\mu})}\right) \right\} \quad (22)$$

are related to Wigner functions *averaged*<sup>25</sup> over the eigenstates of the cluster. For each unstable PO the high- $\ell$  contributions are exponentially damped, and the main contribution to the tunneling rate is given by the  $\ell = 0$  term.

We now have a rigorous criterion for which periodic orbits contribute substantially to the tunneling current in Eq. (20). The injection function  $f_W(y, p_y)$  is centered on  $y_i$  and  $p_y = 0$  with widths  $\sim l_B, \hbar/l_B$  in  $y, p_y$ . From Eqs. 21,22 and the definition of  $\tilde{Q}_\mu$  we find that classical weight functions  $g_\mu$  are centered at  $y_\mu, (p_y)_\mu$  with widths  $\sim l_\mu = \sqrt{2\hbar|m_{12}^\mu|} |4 - \text{Tr}^2[M_\mu]|^{-1/4}$  and  $\hbar/l_\mu$  respectively. When the real and momentum space peaks of these two functions overlap the PO is semiclassically “accessible” and makes a substantial contribution to the tunneling current.<sup>31</sup>

### III. CLASSICAL DYNAMICS

#### A. Model Hamiltonian

The semiclassical formula for the tunneling current, Eq. (20), involves only classical periodic orbits within the well at energies below the top of the barriers. Therefore we can model the system by taking the barriers to be infinite perfectly-reflecting walls at  $z = 0, d$ . With our choice of gauge and coordinates we have

$$H = \frac{(p_x - eBy \cos(\theta) + eBz \sin(\theta))^2}{2m^*} + \frac{p_y^2}{2m^*} + \frac{p_z^2}{2m^*} + eEz + U(-z) + U(z - d) \quad (23)$$

where the functions  $U$  ( $U(z < 0) = 0, U(z > 0) = \infty$ ) represent the infinite walls. Because  $H$  is independent of  $x$ , and  $p_x$  can be eliminated by a gauge transformation<sup>8,2</sup>, this problem can be simplified to a two-dimensional effective hamiltonian<sup>3</sup>. The original hamiltonian involves four variable experimental parameters:  $B, E, \theta, d$  and, as in the case of diamagnetic hydrogen, it is essential to express  $H$  in terms of the minimum number of dimensionless parameters. There are only two energy-independent classical length scales in the problem: the barrier spacing,  $d$ , and  $l_D = (E/B)T_c$ , where  $E/B$  is the drift velocity for perpendicular fields and  $T_c$  is the cyclotron rotation period ( $T_c = 2\pi/\omega_c$ ). Since the length-scale  $d$  will drop out of the problem when the electron energy  $\varepsilon < eEd = eV$  it is natural to scale all lengths by  $l_D$ . When this is done<sup>3</sup> the effective hamiltonian is found to depend on three dimensionless parameters<sup>32</sup>:  $\theta, \beta = 2v_0B/E$  and  $\gamma = \varepsilon/eV$ , where  $v_0$  is the velocity corresponding to the total injection energy  $\varepsilon = m^*v_0^2/2 = \varepsilon_i + eV$ , where  $\varepsilon_i$  is the emitter state injection energy into the well. This energy is typically small compared to  $eV$ . Equally importantly, its ratio to the voltage drop is roughly constant in experimental conditions, implying  $\gamma \approx 1.15$  and constant. Hence for fixed tilt angle the scaled dynamics need only be studied as a function of one parameter,  $\beta$ , which can be regarded as the scaled magnetic field.

#### B. Poincaré Map and the Origin of Chaos

The most convenient surface of section to choose is the plane  $z = d$  corresponding to the collector barrier, as all trajectories within the well impinge on this plane (although in certain cases the emitter SOS may be useful as well). The most convenient phase-space coordinates for the system are the scaled velocities  $v_x/v_0, v_y/v_0$  (we note that for this system  $v_x \sim y$ ). When  $\theta = 0$  the (integrable) motion consists of cyclotron rotation perpendicular to the  $E$  field and uniform acceleration along it (perpendicular to the barriers). Collisions reverse the  $z$ -component of velocity and conserve separately longitudinal and cyclotron energy. When  $\theta \neq 0$  the motion between collisions is still integrable, although now there is a drift velocity added to the cyclotron motion and the acceleration is along the magnetic field with magnitude  $\sim E \cos \theta$ . However collisions now exchange energy between the cyclotron + drift energy and the longitudinal kinetic energy. Since the tilt angle is in the  $y - z$  plane it is straightforward to see that there is no energy exchange at collisions when  $v_y = 0$  and maximal energy exchange when  $v_x = 0$ . This then is the origin of chaos in the system, the energy exchange between the two degrees of freedom depends on the phase of the cyclotron rotation at each collision, very much as in the Chirikov standard map (or kicked rotor)<sup>9</sup>, and just as in that case the system becomes chaotic as this frequency increases relative to the collision frequency (for non-zero tilt angle) - see Fig. 3. Hence as  $B$  increases or  $V$  decreases the system undergoes a transition to global chaos. A simple scaling analysis shows that for fixed  $\gamma$  the classical parameter  $\beta \sim B/\sqrt{V}$ , leading to parabolic curves of constant classical dynamics in the  $B - V$  plane<sup>3</sup>.

In order to derive a simple criterion for the transition to chaos in this system Shepelyansky and Stone<sup>8</sup> noted that, since  $\gamma$  was close to unity, many trajectories would have insufficient longitudinal energy to reach to emitter barrier and



one could consider simply electron motion in the triangular well formed by the electric field and the collector barrier (the “single-barrier” model). In this approximation they showed that the dynamics reduces to an effective standard map with a smooth KAM transition to chaos and a chaos parameter given by  $K = 2\theta\beta$ . When  $K \sim 1$  the last KAM curve of the system breaks and one has full exchange of energy between the degrees of freedom. However our recent work has shown that this approximation does not capture many crucial and interesting aspects of the physics, since those trajectories which *do* reach the emitter barrier are crucial, and including the second barrier changes qualitatively the dynamics in that region of phase space. The single-barrier model is a mathematically tractable and experimentally realizable KAM system; it is studied in detail in ref.<sup>3</sup>. Here we will only consider the double-barrier model relevant to current experiments and to our semiclassical tunneling formula above.

### C. Non-analytic Dynamics in the Double-Barrier Model

The key new feature of the double-barrier model is that the presence of the second barrier introduces non-analytic behavior into the Poincaré map. This map takes the values of  $v_x, v_y$  at a collision and maps them to the values at the subsequent collisions. In the double-barrier model the map defines a closed curve in the SOS corresponding to those initial conditions which reach the second barrier with  $v_z = 0$  exactly. The electron with the initial velocity inside this “critical boundary” reach the second barrier and get an additional “kick”, and otherwise it will not. It is easy to show then that the map will have discontinuous derivatives on this boundary. As a result, just as in the stadium billiard or other systems described by non-analytic maps, the system in the vicinity of the critical boundary undergoes a sudden jump to chaos instead of a smooth KAM transition. However since trajectories sufficiently far from the critical boundary are confined away from the boundary by KAM curves, unlike the stadium one does not have global chaos for arbitrary tilt angle, instead one has a “chaotic halo” region surrounding the critical boundary (see Fig. 4). This region becomes of substantial size well before the phase space becomes globally chaotic and hence has a significant impact on the transition to chaos. We will see below that all of the periodic orbits relevant to the semiclassical tunneling formula are born precisely at the critical boundary in the chaotic halo region. They are born in a novel type of bifurcation we call a “cusp bifurcation” which we will discuss in detail below. These bifurcations were very difficult to detect numerically from the SOS because they violate the bifurcation theorems for analytic hamiltonian maps. Understanding of the short periodic orbits and their bifurcations came from continuity arguments from the  $\theta = 0$  limit and from analytic results to be discussed below.

### D. Periodic Orbits at $\theta = 0$

All periodic orbits can be easily classified at  $\theta = 0$ . First, there is a single isolate “traversing orbit” (TO) which has zero cyclotron energy and follows the line normal to the barriers, bouncing back and forth. Then there are an infinite number of families of “helical orbits” (HO’s) with periods  $T$  given by the resonances between the cyclotron rotation with period  $T_c$  and the longitudinal bouncing-ball motion with period  $T_L$ :

$$T = nT_L = kT_c. \quad (24)$$

In the collector Poincaré map this would define a family of period- $n$  orbits, all related to one another by rotation of the helix. An important point is that when  $\gamma > 1$  (the case we are interested in) there are can be two such families (or “rational tori”) for each pair of integers  $(n, k)$ . For simplicity assume that  $V$  and  $\varepsilon_0$  are fixed and we are varying  $B$ . The resonance condition can then be rewritten as

$$T_L = \frac{2\pi m^* k}{eBn} \quad (25)$$

where  $T_L$  is a function only of the fraction of the total energy which is in the longitudinal motion,  $\varepsilon_L$ . The dependence of  $T_L$  on  $\varepsilon_L$  is shown in Fig. 5. When  $\varepsilon_L < eV$  then  $T_L$  increases as  $\sqrt{\varepsilon_L}$ ; however when  $\varepsilon_L > eV$  then  $T_L$  begins to decrease because the electron reaches the emitter barrier and the bounce returns it faster to the collector barrier. Now consider, for any given resonance  $(n, k)$ , increasing  $B$  from zero. Until  $B_1 \equiv \pi (m^* E)^{1/2} (2ed)^{-1/2} k/n$  there are no solutions for the resonance condition, meaning that the cyclotron rotation is too slow for that particular resonance to occur (here we have used the explicit form of  $T_L(E, d)$ ). For  $B_1 < B < B_2 \equiv B_1 (\sqrt{\gamma} + \sqrt{\gamma - 1})$  there are *two* solutions corresponding to two different families of helical orbits with the same  $T_L$ ; one of which has longitudinal energy greater than  $eV$  and reaches the emitter barrier, the other of which has  $\varepsilon_L < eV$  and doesn’t reach the second barrier (see Fig. 5). We will refer to these two types henceforth as “emitter” and “collector” orbits. As  $B$  is increased further the emitter orbit must *give up* cyclotron energy to remain in resonance, while the collector orbit must *gain*

cyclotron energy in order to remain in resonance. Eventually at  $B = B_2$  the emitter orbit has zero cyclotron energy and is degenerate with the traversing orbit, which exists at all magnetic fields for each energy. For  $B > B_2$  the emitter family of periodic orbits ceases to exist, but the collector family persists for all  $B > B_1$ .

In the surface of section this evolution look as follows (Fig. 6): at  $B_1$  a circle of degenerate period- $n$  orbits appears exactly at the critical boundary (i.e. reaching the emitter barrier with  $v_z = 0$ ). As  $B$  increases this splits into two circles, one with radius greater than the critical boundary (the collector torus) and one with radius smaller (the emitter torus). As  $B$  tends to  $B_1$  the radius of the inner circle shrinks to zero and the torus disappears. The conclusion is that at  $\theta = 0$  all periodic emitter orbits (except the traversing orbit) exist only for a finite interval of magnetic field (and a similar conclusion holds if  $V$  is varied as well). By continuity the same must be true for  $\theta \neq 0$ .

### E. Effect of Non-zero Tilt on Periodic Orbits

Tilting the magnetic field makes the dynamics non-integrable and as usual all families of periodic orbits are destroyed, being replaced by an equal number of stable and unstable isolated fixed points with the same periodicity in the map. Isolated periodic orbits (in this case the traversing orbit) survive the perturbation, and the resonances of these orbits transform into its bifurcations. In ref.<sup>3</sup> we have given an exhaustive analysis of the classical periodic orbit theory in this system. Here we will simply consider briefly the case of period-two orbits which is both illustrative of the general situation and most relevant to the experiments. In particular we will consider the period-two orbits, which occur at the lowest values of magnetic field (these orbits at  $\theta = 0$  make  $1/2$  a cyclotron rotation per collision with the emitter). There are four such orbits, with different topology, the  $(0, 2)_\Lambda$ ,  $(2, 2)_\Lambda$ , and  $(0, 2)_V$ ,  $(2, 2)_V$  orbits (see Fig. 7). The first and second numbers in this notation represent the numbers of bounces per period with the emitter and with the collector respectively, and the subscript describes the “topology” of the orbit.

Since the emitter orbits have different topology they cannot be created together e.g. the  $(2, 2)_\Lambda$  must be created with the  $(0, 2)_\Lambda$  and the  $(2, 2)_V$  with the  $(0, 2)_V$ . Since  $(0, 2)_\Lambda$ ,  $(0, 2)_V$  are collector orbits and  $(2, 2)_\Lambda$ ,  $(2, 2)_V$  are emitter orbits, this can only happen precisely at the critical boundary (just as for the unperturbed case); the bifurcation at which they are born has the non-analytic properties mentioned above which lead to a cusp at the bifurcation point in the bifurcation diagram as shown in Fig. 8. In correspondence to the evolution of tori at  $\theta = 0$  shown in Fig. 6, now as  $\beta$  (or magnetic field) is increased the emitter orbits fixed points move inward in the SOS (but now at slightly different rates for the two different emitter orbits), eventually annihilating with the period-one traversing orbit in successive backwards period-doubling bifurcations. This scenario is general for all emitter orbits: birth at the critical boundary in a cusp bifurcation; death in a backwards bifurcation in the neighborhood of the traversing orbit<sup>33</sup>.

There is an important sub-plot in this scenario. Once the symmetry of the problem has been broken by non-zero tilt angle it is not possible for a  $(2, 2)_V$  and  $(0, 2)_V$  orbit to be born together, because the two “arms” of the  $V$  orbit can no longer be equal in length. Hence the two  $(1, 2)$  orbits are born first, one of which has an arm reaching the emitter barrier and one of which does not. With increasing  $\beta$  the emitter orbit evolves into a  $(2, 2)_V$  orbit, typically not directly, but through a bifurcation “cascade”<sup>34</sup> of the type shown in Fig. 8. In such a cascade a  $(1, 2)$  orbit born in a cusp bifurcation with a  $(0, 2)$  will disappear in a tangent bifurcation with another  $(1, 2)$  orbit born in a cusp bifurcation with a  $(2, 2)$ . Thus the first  $(1, 2)$  orbit is not directly connected by bifurcation to the  $(2, 2)$ , but only indirectly as shown in Fig. 8.

Such bifurcation cascades connected to a resonance of the traversing orbit are a generic feature of this system, for period- $N$  orbits. The only difference is that for the orbits with many bounces in the corresponding bifurcation cascade the “connection” of the  $(0, N)$  and  $(N, N)$  orbits, required by continuity to the behavior at zero tilt angle, is a “multi-step process”, which includes all the “intermediate” periodic orbits of the sequence  $(1, N)$ ,  $\dots$ ,  $(N - 1, N)$ . Thus, despite the increasing complexity, all bifurcation cascades in this system can be analyzed within a single framework.

Each of these bifurcation cascades terminates finally in a resonance with the period-one traversing orbit. The analytic expressions for the period and stability of all period-one orbits, derived in Ref.<sup>3</sup>, provide a straightforward description of each of these resonances, and therefore allow a direct and unambiguous identification of all of the primary bifurcation cascades.

### F. Cusp Bifurcations and Stability Analysis

The existence of both emitter and collector period-one helical orbits at  $\theta = 0$ , which appear together at the critical boundary, implies that for  $\theta \neq 0$  their counterparts must be produced in cusp bifurcations. The analytic analysis of the period-one orbits allowed us to obtain a detailed description of these cusp bifurcations. For example we were able to show that these orbits do not tend to marginal stability at the cusp bifurcation, in contrast to the behavior

required of analytic maps. This led to some more general results on the properties of all CB's, which are as follows: 1) all cusp bifurcations appear at the critical boundary, where the Poincaré map is non-analytic; 2) any cusp bifurcation produces two periodic orbits, which differ by one “point” of contact with the emitter wall; depending on the topology of these orbits, they differ either by one or by two bounces with the emitter barrier per period; 3) out of these two new orbits, the one which has more bounces with the emitter wall (the “more connected” orbit), is “infinitely unstable” ( $\text{Tr}[M] \rightarrow \infty$ ), while its partner might either be stable or unstable.

The calculation of the trace of the monodromy matrix for the  $V$ -type period-2 orbits, presented in the Fig. 9, illustrates the latter point. Note the divergence of the  $\text{Tr}[M]$  for the orbits  $(1, 2)^+$  (the “more connected” partner of  $(0, 2)_V$ ) and  $(2, 2)_V$  (the “more connected” partner of  $(1, 2)^-$ ). Meanwhile, their partners appear either stable ( $(1, 2)^-$ ) or unstable ( $(0, 2)_V$ ).

We hypothesize that the presence of cusp bifurcations with these properties is a general feature of hamiltonian maps with hard wall potentials when the orbits can either hit or miss one part of the hard wall. Therefore the same phenomenology should exist in certain billiard systems (e.g. the “annular billiard”<sup>35</sup>), or in billiards in strong magnetic field<sup>37</sup>, the possibilities we are currently investigating<sup>36</sup>. This phenomenology has importance for the quantum properties of the system, because it leads to special ‘metastable orbits’ as we now discuss in the case of the period-two orbits in the tilted well.

As the effective chaos parameter  $\beta$  increases, the collector orbit  $(0, 2)_V$  becomes increasingly more unstable, as expected for a periodic orbit of a system undergoing the transition from integrability to chaos. However, the other “least connected” orbit of this bifurcation cascade, the orbit  $(1, 2)^-$ , shows a dramatically different behavior. Initially, with the increase of  $\beta$  it loses stability, as expected. However, this orbit will later have to annihilate with the orbit  $(1, 2)^+$  in a backwards tangent bifurcation. Since the tangent bifurcation can only involve two marginally stable orbits, the initially stable  $(1, 2)^-$  can not develop strong instability and must stay either stable or only marginally unstable in its whole interval of existence.

Note, that this continuity argument applies to any “intermediate” period orbit, which appears as the “less connected” partner in a cusp bifurcation, and annihilates in a tangent bifurcation. Therefore, there must be at least one such metastable orbit in any primary bifurcation cascade of this system. This “metastability” of a certain subset of the classical periodic orbits in the quantum well in a tilted magnetic field has profound consequences in its quantum spectrum.

## G. The Origin of Strong Scarring

It is now well known that certain quantum wavefunctions of classically chaotic systems can strongly localize near unstable periodic orbits. Such wavefunctions are termed “scars” and their properties have been extensively studied and well understood during the last decades<sup>38–41</sup>. The scarred wavefunction are most likely to be associated with the periodic orbits which are not too unstable. A sufficient condition of the strong scarring is  $\lambda T \lesssim 1$ , where  $\lambda$  is the instability (Lyapunov) exponent associated with the orbit, and  $T$  is its period. Typically, in chaotic systems, the periodic orbits quickly become increasingly more unstable, as the classical parameter driving the system to chaos, is increased. Such orbits can strongly scar the wavefunctions only in a small interval of classical parameter space in which they are not too far from stability.

Therefore, it came as a surprise, when a persistent scarring by the same orbit in a large interval of applied voltage, was observed both numerically<sup>6</sup> and (indirectly) experimentally<sup>7</sup>. Although it has been argued<sup>42</sup> (with some merit in our view) that the experimental results are in a regime of low quantum numbers for which the concept of scarring becomes ambiguous, extensive quantum numerical calculations confirm a strong periodic scarring at high quantum numbers as well. This phenomenon is naturally explained by the “metastability” of the “intermediate” periodic orbits in this system. Since these orbits remain close to stability over their whole interval of existence, they produce strong scars in the quantum wavefunctions in a large interval of the applied voltage or magnetic field. This behavior is illustrated in Fig. 10, which represents the calculation of the scar “strength” (defined as the value of the Husimi projection of the quantum wavefunction, taken at the fixed point the periodic orbit<sup>43</sup>) due to the  $(1, 2)^-$  orbit.

As we already pointed out, there is at least one “metastable” orbit in each of the primary bifurcation cascades. The semiclassical theory therefore implies that each of these orbits should also produce strong scars in quantum wavefunctions. Indeed, a detailed analysis<sup>4</sup> of the wavefunctions in the quantum well uncovers strong and persistent scarring due to the “metastable” period-3 orbit  $(1, 3)$  and period-5 orbit  $(1, 5)$ .

## H. “Exchange Interaction” between Bifurcation Cascades

An interesting feature of the classical dynamics in the quantum well in a tilted magnetic field, noted in Ref.<sup>4</sup>, is the exchange bifurcations between the orbits of the different primary bifurcation cascades. Fig. 11 depicts the exchange bifurcation between  $V$ -type periodic orbits of two different period-2 cascades. For convenience of the further analysis, we represent the relevant orbits by the  $x$ -components of the velocity  $v_x \propto y$  at the *emitter* barrier (by definition, such diagrams do not show the collector orbits). As the tilt angle approaches the critical value of  $\theta^* \approx 30^\circ$ , the orbits  $(1, 2)^-$  and  $(1, 2)^+$  of the first cascade, and the orbit  $(1, 2)_*^+$  of the second cascade come close to each other, and at the critical angle exchange partners, so that for  $\theta > \theta^*$  the orbit  $(1, 2)_*^+$  is now paired with  $(1, 2)^-$  and belongs to the first cascade, whereas the orbit  $(1, 2)^+$  is paired with  $(1, 2)_*^-$  and belongs to the second cascade. As the tilt angle is increased further, the two reconfigured bifurcation cascades move away from each other - see Fig. 11c.

## IV. SEMICLASSICAL TUNNELING SPECTRA AND COMPARISON WITH EXPERIMENT AND NUMERICAL CALCULATIONS

### A. Periodic Orbit Theory

Since the motion of the fixed points of the relevant periodic orbits near the exchange bifurcation strongly affects their accessibility for tunneling, the exchange bifurcation dramatically manifests itself in the tunneling spectra. This is demonstrated in Fig. 11, where the gray-scale regions (calculated at  $B = 8T$ ) represent the semiclassical width  $l_\mu$  of these wavefunctions localized near the corresponding periodic orbits. The width of the injection function  $f_W(y)$  is represented by the region between dashed lines. Whenever these regions overlap for some value of  $\beta$  the orbit is accessible and Eq. (20) predicts that a peak-doubling region will appear in the  $B - V$  parameter space along the parabola corresponding to that value of  $\beta$  (see Fig. 12)<sup>44</sup>.

At  $\theta = 29^\circ$  the accessibility intervals for the  $(1, 2)^-$  orbit and the  $(1, 2)_*^+$  orbit cover the entire interval  $4.3 < \beta < 10.9$  overlapping briefly around  $\beta = 7.5$ . Thus one expects a large region of peak-doubling in the  $B - V$  plane with no gaps as observed in the experiment<sup>2</sup>. Since the periods of the relevant orbits are almost degenerate, these distinct periodic orbits will produce the oscillations of the tunneling current of almost the same frequency. Note, that the orbits  $(1, 2)^-$  and  $(1, 2)^+$  of the first cascade are slightly better coupled with the emitter state, that the orbit  $(1, 2)_*^+$ . Therefore, in the I-V, we expect the amplitude of oscillations to be higher in the high-voltage region ( $\beta \sim 1/\sqrt{V}$ ).

As  $\theta = 31^\circ$ , immediately after the exchange bifurcation, the relevant orbits of the newly-formed “first cascade” start to move away from the accessibility region. As a result, the amplitude of the oscillations of the tunneling current is now higher in the low-voltage region, and we expect an abrupt amplitude change around  $\beta \approx 7.3$ , ( $V \approx 0.44V$  for  $B = 8T$ ). This is observed clearly in the experimental data of Fig. 12(a),(d), where the amplitude change is compared to theory. The theory is found to predict the ratio of the amplitudes between the low and high voltage regions (above 0.45V) with only 25% mean error.

At  $\theta \approx 34^\circ$ , the periodic orbits of the first cascade are no longer accessible. At the same time the  $(1, 2)^+$  orbit is still highly accessible at low voltages (high  $\beta$ ). Thus we expect the high voltage oscillations to disappear at  $\theta = 34^\circ$  while the low voltage oscillations persist. This is seen clearly in Fig. 12, again in good qualitative and quantitative agreement with theory.

In Fig. 12, we plot the peak position data of Ref.<sup>5</sup> in the entire  $B - V$  plane against the semiclassical prediction based on the contributions of these periodic orbits. Again, the comparison shows a good agreement between semiclassical calculation and the experimental data<sup>45</sup>.

### B. Beyond Periodic Orbits: The Closed Orbit Theory

As was demonstrated in the previous section, the periodic theory can be successfully used for the quantitative description of the tunneling spectra over a wide range of system parameters. However, the periodic orbit approach may fail near the bifurcations, when the relevant orbits are not isolated, and the second-order expansion, used to obtain the POF, is not justified. A manifestation of this can be seen in Fig. 12a,d, where one sees a spurious dip in the semiclassical trace near  $V = 0.3V$  which has no analog in the experimental  $I - V$  curve. This dip is precisely due to the occurrence of a bifurcation near this voltage. Also, the POF provides no description for the “ghost effect” near tangent bifurcations, when the contribution of the particular orbits which disappear in the bifurcation remains in the spectrum even after their disappearance<sup>16</sup>.

Generally, the regions where the POF is inadequate, are *semiclassically small*, i.e. the corresponding intervals  $\Delta V, \Delta B \sim \hbar$ . And in the case of the ghost effect, the ghost contributions decay exponentially away from the bifurcation point. However, due to a relatively large value of the effective  $\hbar$  in the experiment<sup>1,2,7</sup> (particularly in Ref.<sup>7</sup>), the measured tunneling spectra do show clear features related to these effects. In particular, as it has been shown by Monteiro et al.<sup>10</sup> that a substantial part of the peak-doubling region at  $\theta = 27^\circ$  is due to the ghost of the (1, 2) orbit, and the period-1 oscillations at high magnetic field at  $\theta = 11^\circ$  are related to the ghost of (1, 1) orbit.

Previously the “ghost” contributions have been calculated using an extension of the actual classical dynamics to the complex space. In this approach, after a real periodic orbit “dies” in a bifurcation, a counterpart orbit continues to exist in complex space-time. The imaginary part of the action of this complex periodic orbit describes the exponential damping of it’s contribution in the density of states<sup>16</sup>.

Very recently, it has been shown, that complex dynamics can be successfully used for the quantitative description of the tunneling current<sup>17</sup>. A full stationary phase condition, when applied directly to Eq. (8), leads to *non-periodic* and *complex* orbits. These trajectories were shown to smoothly “interpolate” between successive relevant periodic orbits, also providing an excellent quantitative description of the tunneling current in the “ghost” regime.

However, the approach of Ref.<sup>17</sup> does not possess one of the important advantages of the semiclassical theory described in the present work - the separation of the “isolated” subsystems of the quantum well and the emitter state. In the approach of<sup>17</sup> a different emitter state leads to a completely different set of complex trajectories, which enter the final expression for the tunneling current.

The Closed Orbit Formula derived in the present paper ( Eq. (14) ) has the advantages that it only involves real orbits within the well, which depend on the emitter state only weakly (through the location of the injection point  $y_i$ ). It is therefore of interest to see if a semiclassical formula with this rather different structure can also describe the ghost effect in the tunneling spectra quantitatively.

The relations (13),(14) provide a complete description of all the ghost contributions in the tunneling spectra. For simplicity here we will apply them to self-retracing orbits (the most relevant to experiment) and introduce a further approximation to re-express the injected orbit in terms of the closed orbit with the minimum  $\Delta p_y$ .

As it was argued in Section II.C, an injected orbit can substantially contribute to the tunneling current only if the change of momentum  $\Delta p_y$  after returning to the injection point is small. Consider such an injected orbit when it is near a tangent bifurcation as shown in Fig. 2. Just before the bifurcation there exist no periodic orbit in a semiclassically small neighborhood of the injected orbit, but there does exist a unique nearby orbit of minimal  $\Delta p_y$ . This orbit is determined by the classical dynamics in the well and not by the injection point, so we prefer to express the semiclassical tunneling current in terms of its properties, rather than those of the injected orbit. Let its point of contact with the emitter be at  $y_0$ , where  $|y_0 - y_i|$  is semiclassically small by assumption; than the change of momentum of the injected orbit<sup>46</sup> can be expressed as

$$\Delta p_y = 2p_y^0 + K_0 (y_i - y_0)^2, \quad K_0 \equiv \left. \frac{\partial^2 p_y}{\partial y^2} \right|_{y=y_0} \quad (26)$$

Assuming that the electrons in the emitter (or collector) are in the lowest Landau level, for the corresponding ghost contribution to the tunneling rate we obtain:

$$W_{\text{ghost}} = A_{\text{gh}}^{\text{sc}} \exp\left(-\frac{t_0}{\tau_{\text{opt}}}\right) \cos\left(\frac{S_0}{\hbar} + \phi_0\right) \quad (27)$$

where

$$A_{\text{gh}}^{\text{sc}} = A_0 \exp(-\xi^2) \quad (28)$$

$$A_0 = \frac{4}{m^*} \frac{p_z^0}{\left[1 + \left(\frac{m_{12}^0 \hbar}{2l_B^2}\right)^2\right]^{1/4}} \exp\left[-(p_y^0 l_B / \hbar)^2\right], \quad (29)$$

$$\xi = \left[ \frac{\left(p_y^0 + K_0 (y_i - y_0)^2\right)^2}{1 + \left(K_0 (y_i - y_0) \frac{l_B^2}{2\hbar}\right)^2} - (p_y^0)^2 \right]^{1/2} \frac{l_B}{\hbar}, \quad (30)$$

$m_{ij}^0$ ,  $t_0$  and  $S_0$  are respectively the monodromy matrix, the traversal time and the action of the closed orbit with minimum change of momentum  $\Delta p_y$ , and the  $\phi_0$  is the corresponding phase, which, in addition to the constant part,

related to the topological index of the orbit, has also a smoothly varying component. Although it is straightforward to obtain the latter from (14), the result is somewhat complicated, and is not presented here. Note, that the classical input for the Eq. (27) depends again only on the injection point and not on the particular emitter state.

Thus in Eq. (27) we have derived a relatively simple explicit formula for the ghost contributions in the tunneling spectrum in terms of the classical properties of the closed orbit with minimal values of  $\Delta p$  ( $\equiv 2p_y$  for a self-retracing closed orbit). Note that the strength of the ghost contribution is exponentially small in  $(\Delta p/p_B)^2$ , where  $p_B = \hbar/l_B \sim \sqrt{\hbar}$ .

Now we proceed with a detailed numerical test of the “ghost formula” (27). Note that in principle the expression (27) can describe the tunneling rate both from the ground Landau level in the emitter to the well *or* from the well to the ground Landau level in the collector. Although the actual experimental tunneling current in the incoherent regime does not depend on the latter quantity, either can be used to test the validity of Eq. (27) in the ghost regime. In fact the tunneling rate into the collector is a more convenient object for numerical computation since it is non-zero for energies less than  $eV$  and thus can be expressed in terms of lower-lying eigenstates for interesting value of  $eV$ . Effectively then we will test the formula in the single-barrier model which we studied in detail in reference<sup>3</sup> for which the classical dynamics depends only on  $\beta$ . The first (as a function of  $\beta$ ) relevant bifurcation in that model is the tangent bifurcation of the period-one orbits which we designated  $(0, 1)^{+(1)}$  and  $(0, 1)^{-(1)}$  (for a detailed description of the corresponding classical dynamics, see Ref.<sup>3</sup>, Section III.C). We will now consider the “ghost” related to that tangent bifurcation at  $\theta = 11^\circ$ . Although for any given system parameters  $y_i$  and  $y_0$  are fixed in Eq. (27), for a complete test of the formula we treat  $y_i$  as an independent variable and study the amplitude  $A_{\text{gh}}^{\text{sc}}$  as a function of both  $y_i$  and  $\beta$  ( $\sim \sqrt{\varepsilon}$ ).

In Fig. 13 we show the comparison of the exact and semiclassical results for  $A_0$ . With *no fitting parameters* the semiclassical calculation (represented by a dashed line in Fig. 13) is in a good agreement with exact data (open circles). However, essentially perfect agreement can be obtained when one introduces a single fitting parameter by means of the definition  $A_0^{\text{sc}}(\varepsilon_L)$  where the “longitudinal energy”  $\varepsilon_L$  is defined as  $\varepsilon_L \equiv \varepsilon - \kappa\hbar\omega_c$ , with the  $\kappa \lesssim 1$  being the fitting parameter.

The quantity  $\kappa\hbar\omega_c$  can be interpreted as the energy of the motion transverse to the direction of the periodic orbit. As was shown in Section II.C, a careful consideration of the higher-period orbits, related to the repetitions of the short trajectories, leads to the replacement of the total energy by it’s longitudinal part in the *phase* of the corresponding contribution to the tunneling rate. It is natural to assume, that such a replacement should take place in *both* the phase *and* the amplitude. However, because the transverse energy  $\varepsilon_\perp \sim \hbar$ , the correction to the amplitude is of the next order in  $\hbar$ , and is not captured by the semiclassical theory. The calculation, presented in Fig. 13 gives a clear indication that the amplitude should also, in fact, depend on the *longitudinal* energy.

As follows from (27), neglecting the slowly varying prefactor, the amplitude depends only on the “scaled deviation” from it’s maximum value  $\xi$ :

$$A_{\text{gh}}^{\text{sc}}(y_i, \beta) \sim \exp \left[ -\xi(y_i, \beta)^2 \right] \quad (31)$$

In Fig. 14 we plot the scaled amplitude as a function of  $\xi$  for eight different values of  $\beta$ , and a good agreement is found with the predicted form (31). Note, that since the formula (27) is, in turn, also based on the expansion near the contact point  $y_0$  of the “minimum  $\Delta p_y$  closed orbit”, the deviation of the exact data from (31) should increase for larger  $\xi$ , again in agreement with the calculation presented in Fig. 14.

## V. CONCLUSIONS

In the work which we have concluded with the present paper, we have developed a complete semiclassical theory of resonant tunneling in quantum wells in a tilted magnetic field. The theory was shown to be in good qualitative and quantitative agreement with the experiments of Muller et al<sup>2</sup>, and explains many puzzling features of the tunneling spectra. In particular we have explained the phenomenon of persistent scarring of wavefunctions in terms of the properties of cusp bifurcations and bifurcations cascades, which lead to metastable periodic orbits. We expect these concepts to extend to other systems and for the same persistent scarring to be found in such systems in the appropriate parameter ranges. Furthermore we have demonstrated explicitly the possibility of describing quantitatively the ghost contributions of vanished periodic orbits in terms of a semiclassical theory of real closed orbits.

The authors wish to thank G. Boebinger, D. Shepelyansky, T. S. Monteiro, T. M. Fromhold, H. Mathur, G. Hackenbroich and J. Delos for helpful discussions. We further thank T. S. Monteiro for communicating the results of recent work on the semiclassical formulas and their extension to complex orbits prior to publication. This work was partially supported by NSF Grant No. DMR-9215065.

## APPENDIX A: SEMICLASSICAL GREEN FUNCTION NEAR A RECTANGULAR BARRIER

The equation (5), used for the calculation of the tunneling rate from the emitter to the well, requires the knowledge of the normal derivative of the Green function  $\partial_{z_1}^2 G(y_1, z_1 = 0; y_2, z_2 = 0)$ . Because of the apparent discontinuity of the potential *exactly* where the Green function is evaluated, the semiclassical approximation for this object should be performed with care.

First, we consider the first derivative  $\partial_{z_1} G(y_1, z_1 = 0; y_2, z_2)$ , which we define as

$$\frac{\partial G(y_1, z_1 = 0; y_2, z_2)}{\partial z_1} = \lim_{z_1 \rightarrow 0} \frac{\partial G(y_1, z_1; y_2, z_2) - G(y_1, 0; y_2, z_2)}{z_1} \quad (\text{A1})$$

The value  $z_1 \rightarrow +0$  should be *classically small* (e.g.  $z_1 \sim \hbar$ ), so that the change of the smooth part of the total potential  $V(y, z)$  at the distance  $z_1$  is small compared to the kinetic energy of the electron.

When  $z_1 \neq 0$ , the semiclassical Green function can be expressed as a sum over classical trajectories<sup>20</sup> (indexed by  $\nu$ ) connecting the points  $(y_1, z_1)$  and  $(y_2, z_2)$ :

$$G = \frac{2\pi}{(2\pi i \hbar)^{3/2}} \sum_{\nu} \sqrt{|D_{\nu}|} \exp\left(\frac{i}{\hbar} S_{\nu} - \frac{i\pi\mu_{\nu}}{2}\right) \quad (\text{A2})$$

where  $D$  is the (semi)classical amplitude,  $S$  is the action integral and  $\mu$  is the topological index of the trajectory  $\nu$ .

When the starting point  $(y_1, z_1)$  is near the emitter barrier, the Green function can be expressed in terms of the classical trajectories starting *at* the emitter barrier - i.e. from the point  $(y_1, 0)$ . For each such trajectory  $j$  there are *two* trajectories  $j_1$  and  $j_2$  [starting from  $(y_1, 1)$ ] with different number of collisions with the barrier, which collapse to  $j$  when  $z_1 \rightarrow 0$  - see Fig. 15. In the semiclassical limit we have:

$$\begin{aligned} S_{j_1} &= S_j - p_z^{(1)} z_1, & S_{j_2} &= S_j + p_z^{(1)} z_1, \\ \mu_{j_1} &= \mu_j, & \mu_{j_2} &= \mu_j + 2 \end{aligned} \quad (\text{A3})$$

where  $\mathbf{p}^{(1)}$  the electron momentum at the starting point, and the extra 2 in the expression for  $\mu_{j_2}$  corresponds the phase increment of  $\pi$  due to an additional (with respect to the trajectory  $j$ ) reflection from the hard wall.

Substituting (A3) into (A2), we obtain:

$$G(y_1, z_1; y_2, z_2) = \frac{4\pi i}{(2\pi i \hbar)^{3/2}} \sum_j \sqrt{|D_j|} \sin\left(\frac{p_z^{(1)} z_1}{\hbar}\right) \exp\left(\frac{i}{\hbar} S_j - \frac{i\pi\mu_j}{2}\right) \quad (\text{A4})$$

and therefore the first normal derivative

$$\left. \frac{\partial G(y_1, z_1; y_2, z_2)}{\partial z_1} \right|_{z_1=0} = \frac{4\pi i}{(2\pi i)^{3/2} \hbar^{5/2}} \sum_j p_z^{(1)} \sqrt{|D_j|} \exp\left(\frac{i}{\hbar} S_j - \frac{i\pi\mu_j}{2}\right) \quad (\text{A5})$$

Using a similar approach, one can show, that the second derivative

$$\left. \frac{\partial^2 G(y_1, z_1; y_2, z_2)}{\partial z_1 \partial z_2} \right|_{z_1=z_2=0} = \frac{8\pi i}{(2\pi i)^{3/2} \hbar^{7/2}} \sum_j p_z^{(1)} p_z^{(2)} \sqrt{|D_j|} \exp\left(\frac{i}{\hbar} S_j - \frac{i\pi\mu_j}{2}\right) \quad (\text{A6})$$

where  $\mathbf{p}_z^{(1)}$  and  $\mathbf{p}_z^{(2)}$  are respectively the initial and the final momenta.

<sup>1</sup> T. M. Fromhold *et al*, Phys. Rev. Lett. **72**, 2608 (1994);

<sup>2</sup> G. Muller *et al*, Phys. Rev. Lett. **75**, 2875 (1995)

<sup>3</sup> E. E. Narimanov and A. D. Stone, Phys. Rev. B **57**, 9807 (1998); also preprint cond-mat/9704083.

<sup>4</sup> E. E. Narimanov and A. D. Stone, Phys. Rev. Lett. **80**, 49 (1998); also preprint cond-mat/9705167.

<sup>5</sup> E. E. Narimanov and A. D. Stone, Phys. Rev. Lett. **80**, 4024 (1998); also preprint cond-mat/9707073.

- <sup>6</sup> T. M. Fromhold *et al*, Phys. Rev. Lett., **75**, 1142 (1995).
- <sup>7</sup> P. B. Wilkinson *et al*, Nature, **380**, 608 (1996).
- <sup>8</sup> D. L. Shepelyansky and A. D. Stone, Phys. Rev. Lett. **74**, 2098 (1995).
- <sup>9</sup> B. V. Chirikov, Phys. Rep. **52**, 263 (1979).
- <sup>10</sup> T. S. Monteiro *et al*., Phys. Rev. E **53**, 3369 (1996); Phys. Rev. B **56**, 3913 (1997).
- <sup>11</sup> D. S. Saraga and T. S. Monteiro, Phys. Rev. E **57**, 5352 (1998).
- <sup>12</sup> T. M. Fromhold *et al*, Phys. Rev. B, **51**, 18029 (1995)
- <sup>13</sup> E. Bogomolny and D. Rouben, cond-mat/9801171 . Two semiclassical formulas are discussed in this work, with primary emphasis on the one analyzed in<sup>11</sup> which does not take into account the variation of the emitter state wavefunction on the semiclassical scale  $\sim \sqrt{\hbar}$ .
- <sup>14</sup> D. S. Saraga, T. S. Monteiro, and D. C. Rouben, preprint chao-dyn/9806007.
- <sup>15</sup> Although the “width” of such regions in the parameter space is “semiclassically” small, it was shown<sup>10</sup>, that at  $\theta = 27^\circ$  the “ghost” effect is responsible for a substantial part of the experimentally seen peak-doubling.
- <sup>16</sup> A. M. Ozorio de Almeida and J. H. Hannay, J. Phys. A **20**, 5873 (1987).
- <sup>17</sup> D. S. Saraga and T. S. Monteiro, preprint chao-dyn/9806012.
- <sup>18</sup> M. C. Payne, J. Phys. C : Solid State Phys. **19**, 1145 (1986)
- <sup>19</sup> J. Bardeen, Phys. Rev. Lett. **6**, 57 (1961).
- <sup>20</sup> M. C. Gutzwiller, *Chaos in Classical and Quantum Mechanics* (Springer-Verlag, New York, 1990)
- <sup>21</sup> Typically in the experiments  $U_0 \simeq 1. - 1.5$  eV, while the injection energy  $\varepsilon_i \sim 10 - 100$  meV and the cyclotron energy  $\hbar\omega_c < 50$  meV.
- <sup>22</sup> In this representation, the dependence of the matrix element on the barrier height  $U_0$  is carried by the wavefunctions of the isolated emitter, calculated at  $z = 0$ .
- <sup>23</sup> T. Ando *et al*, Rev. Mod. Phys. **54**, 437 (1982).
- <sup>24</sup> This does not include the zero-length trajectories, which contribute to the *smooth* part of  $W$  (so called “Weyl term”) and are not relevant for the *oscillatory* part of the tunneling rate.
- <sup>25</sup> M. V. Berry, Proc. Roy. Soc. Lond. A **423**, 219 (1989).
- <sup>26</sup> M. L. Du and J. B. Delos, Phys. Rev. Lett. **58**, 1731 (1987); Phys. Rev. A **38**, 1896 (1988).
- <sup>27</sup> This stationary phase integration was however used by Bogomolny and Rouben in<sup>13</sup> to obtain a simplified analytical formula for the tunneling current. In Ref.<sup>11</sup> this formula was shown to give only poor agreement with exact calculations and experimental data as we would expect from the arguments presented in the text.
- <sup>28</sup> E. E. Narimanov and A. D. Stone, unpublished.
- <sup>29</sup> H. Schromerus and F. Haake, preprint chao-dyn/9703016.
- <sup>30</sup> W. H. Miller, *J. Chem. Phys.* **63**, 996 (1975).
- <sup>31</sup> The semiclassical formula of Eq. (20) breaks down at bifurcations, when the periodic orbits are not isolated. Correspondingly, the semiclassical width can either diverge or vanish (depending on the nature of the bifurcation). These divergences are spurious but are integrable in Eq. (20) and only lead to inaccuracies in a small interval of  $\beta$  very close to the bifurcation. In these intervals one should use the Closed Orbit Formula.
- <sup>32</sup> This representation was introduced in Ref.<sup>3</sup>. Alternative scaling relations were used in Refs.<sup>2,8,10</sup>.
- <sup>33</sup> Unlike their birth in cusp bifurcations, all emitter orbits “die” in analytic backwards bifurcations which follow the generic rules of hamiltonian bifurcation theory. Hence, for example, backwards bifurcations with the period-one traversing orbit is allowed for period-two orbits, but not for period-three orbits, which vanish near the traversing orbit in a tangent bifurcation according to the “touch-and-go” scenario described in ref.<sup>26</sup>.
- <sup>34</sup> These bifurcation cascades which connect various orbits with the *same* period but different topology are not to be confused with the well-known period-doubling sequences connecting orbits of successively longer period.
- <sup>35</sup> O. Bohigas, S. Tomsovic, and D. Ullmo, Phys. Rep. **223**, 43 (1993); O. Bohigas, D. Boose, R. Eglydio de Carvalho, and V. Marvulle, Nucl. Phys. A **560**, 197 (1993).
- <sup>36</sup> E. E. Narimanov and A. D. Stone, unpublished.
- <sup>37</sup> J. Blaschke and M. Brack, Physica E **1**, 288 (1997).
- <sup>38</sup> E. J. Heller, Phys. Rev. Lett **53**, 1515 - 1518 (1984).
- <sup>39</sup> O. Agam and S. Fishman, Phys. Rev. Lett **73**, 806 (1994).
- <sup>40</sup> S. Fishman, B. Georgeot, and R. E. Prange, Journal of Phys. A **29**, 919 (1996).
- <sup>41</sup> L. Kaplan and E. J. Heller, Annals of Physics **264**, 171 (1998).
- <sup>42</sup> T. S. Monteiro, D. Delande, and J. P. Connerade, Comment, Nature **387**, 863 (1997).
- <sup>43</sup> The definition of the “scar strength” is not unique, e.g. one may instead integrate the modulus of the wavefunction along the periodic orbit in the real space<sup>49</sup>. The difference in the definition, however, will not affect the qualitative difference between “localized” and “ergodic” states.
- <sup>44</sup> Note, that for all these orbits at the point of collision with the emitter barrier  $p_y = 0$ .
- <sup>45</sup> The major remaining discrepancy, that the experimental peak-doubling regions are observed at lower voltages than calculated by the semiclassical theory, arises from an offset voltage in the sample<sup>2</sup> and band non-parabolicity effects<sup>12</sup>.
- <sup>46</sup> For simplicity, here we consider the case of a family of *self-retracing* orbits.



- <sup>47</sup> L.Reichl, *The Transition to Chaos in Conservative Classical Systems : Quantum Manifestations* (Springer-Verlag, New York, 1992).
- <sup>48</sup> Actually the scar strength turns on *before* the tangent bifurcation signalling the birth of the orbit due to the existence of “ghost” orbits<sup>16</sup>.
- <sup>49</sup> D. Wintgen and A. Hönig, Phys. Rev. Lett. **63**, 1467 (1989).

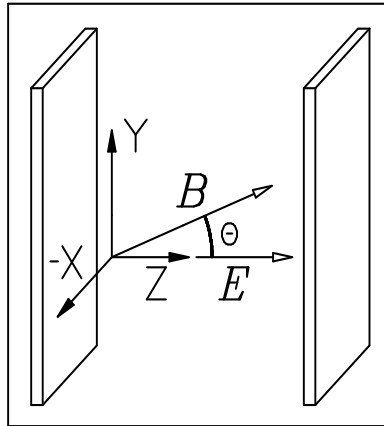


FIG. 1. Schematic of the geometry and coordinate system used in this work

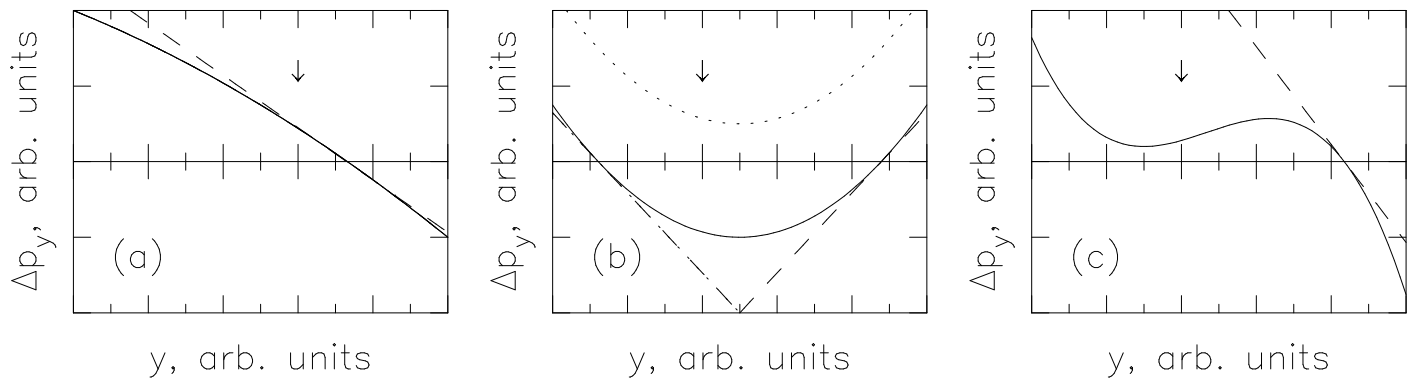


FIG. 2. The change of momentum  $\Delta p_y$  for the closed orbits of a particular family, as a function of “starting coordinate”  $y$ . The dashed lines show the linear approximation for  $\Delta p_y$ , used in (16), (17). The arrow indicates the “injection point”  $y = y_i$ . If at  $y = y_i$  the value of  $\Delta p_y$  is small, the linear approximation is justified (a), but fails in the vicinity of a bifurcation (b),(c). In (b) the dotted and solid lines respectively represent the behavior before and after a tangent bifurcation.

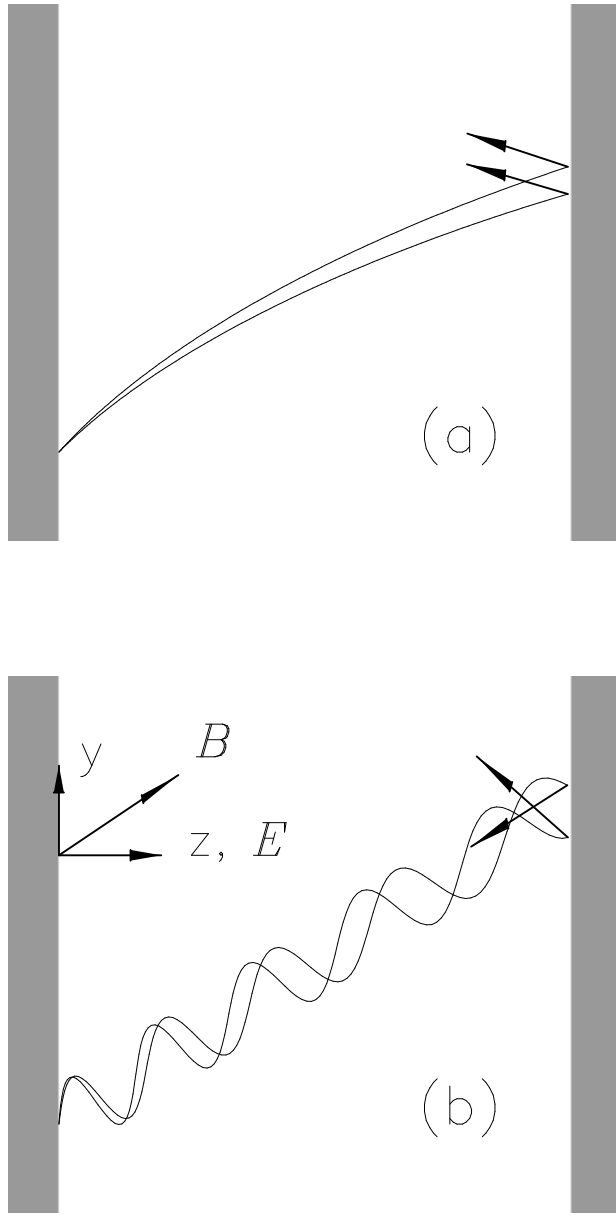


FIG. 3. The evolution of two classical trajectories, started from the same point at the emitter barrier with almost identical velocities, for (a)  $\omega_c\tau \lesssim 1$ , and (b)  $\omega_c\tau \gg 1$ , where  $\tau$  is the well traversal time. The black arrows represent the velocities immediately after collision with the collector barrier; the inset shows the directions of the magnetic and electric fields, and the coordinate system. Note the large amplification of small differences when the cyclotron rotation rate is large compared to the traversal time. This is the origin of chaos in the system, as discussed in the text.

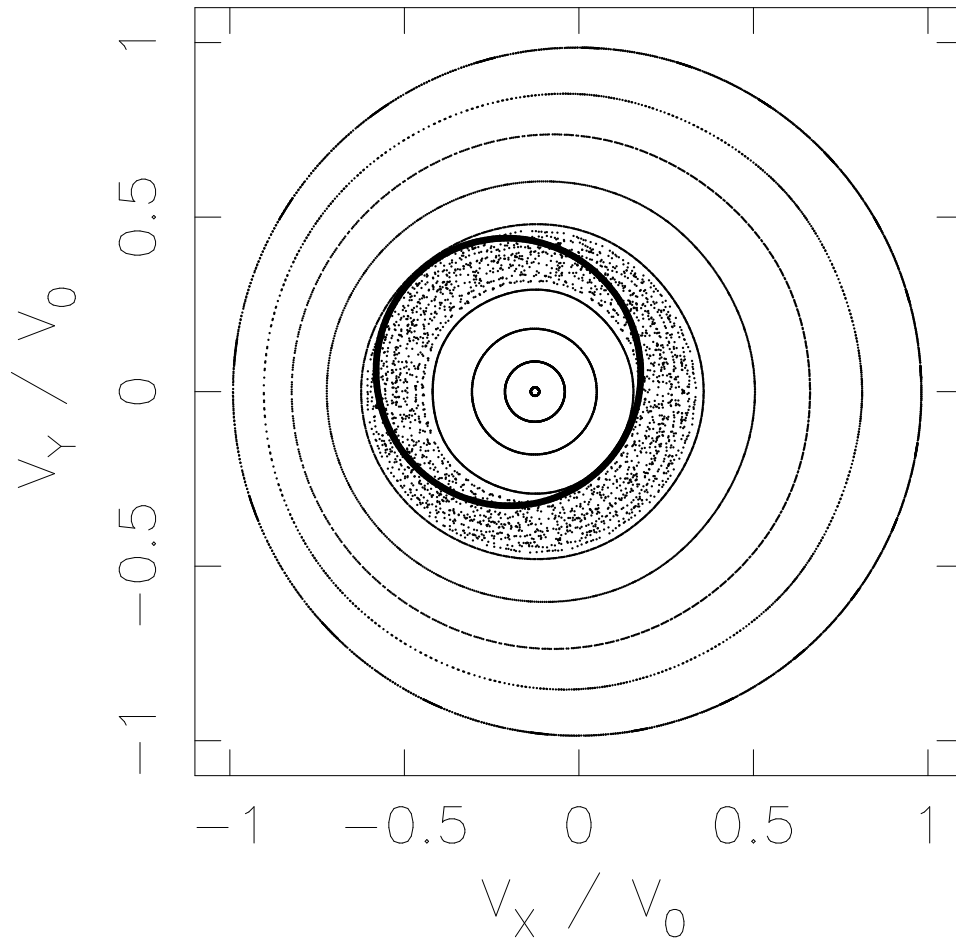


FIG. 4. The “chaotic halo” near the critical boundary (thick solid line), created by nonanalyticity of the Poincare map, seen at the collector barrier surface of section at  $\beta = 2$ ,  $\gamma = 1.17$  and  $\theta = 30^\circ$ . Note that the halo region in which trajectories can hit the emitter barrier intermittently is highly chaotic while the inner and outer regions, where trajectories either always hit or always miss the emitter, are still quite regular. All the periodic orbits relevant to the tunneling current are born at the critical boundary and then move inwards.

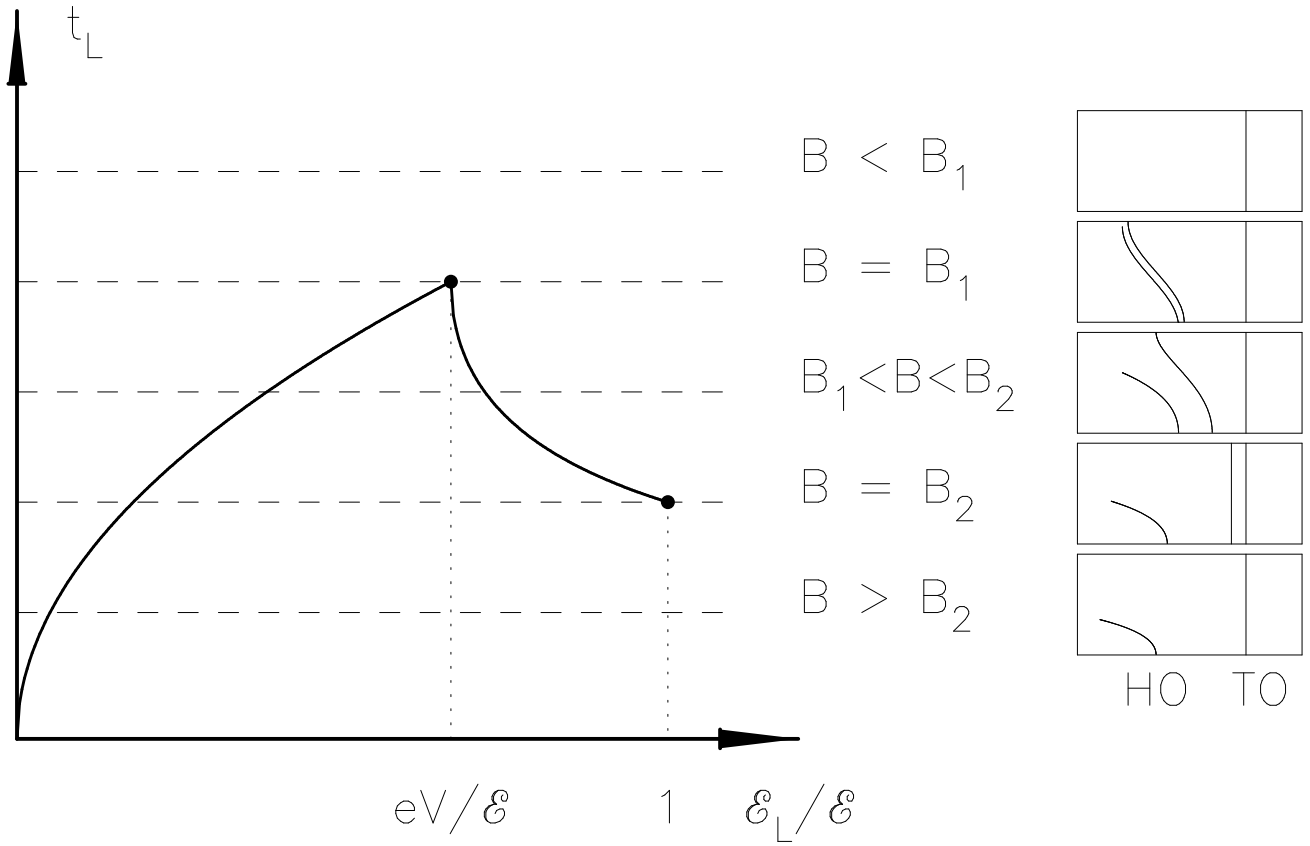


FIG. 5. The dependence of the traversal time of longitudinal motion  $t_L$  on the fraction of the total energy which is longitudinal,  $\epsilon_L/\epsilon$ . The dashed lines represent the three different regimes discussed in the text,  $B < B_1$ ,  $B_1 < B < B_2$ ,  $B > B_2$  and the corresponding borders  $B = B_1$  and  $B = B_2$ . The insets on the right schematically represent the different periodic orbits in each regime.

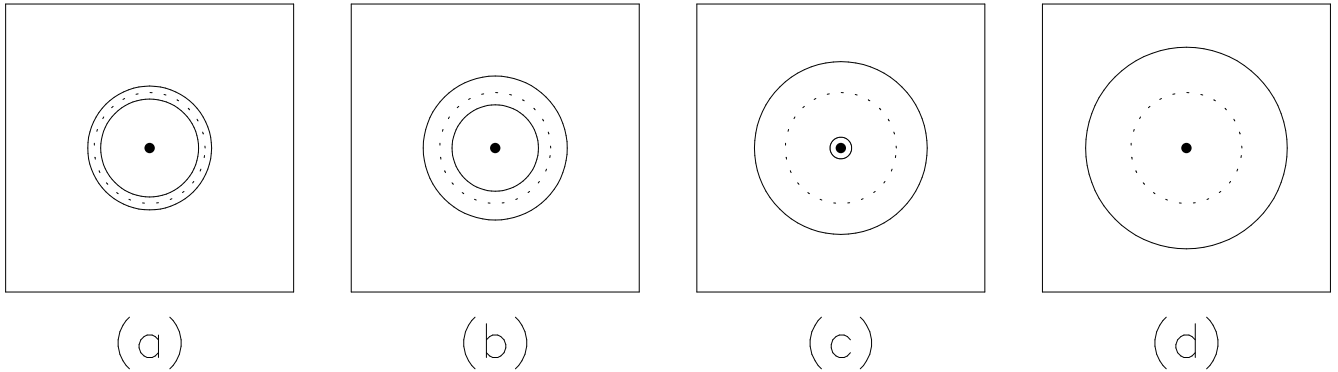


FIG. 6. The schematic representation of the tori at the Surface of Section at (a)  $B = B_1 + \epsilon$ , (b)  $B_1 < B < B_2$ , (c)  $B = B_2 - \epsilon$ , (d)  $B > B_2$ ,  $\epsilon \rightarrow +0$ . Dotted circle represents the critical boundary at  $\theta = 0$ .

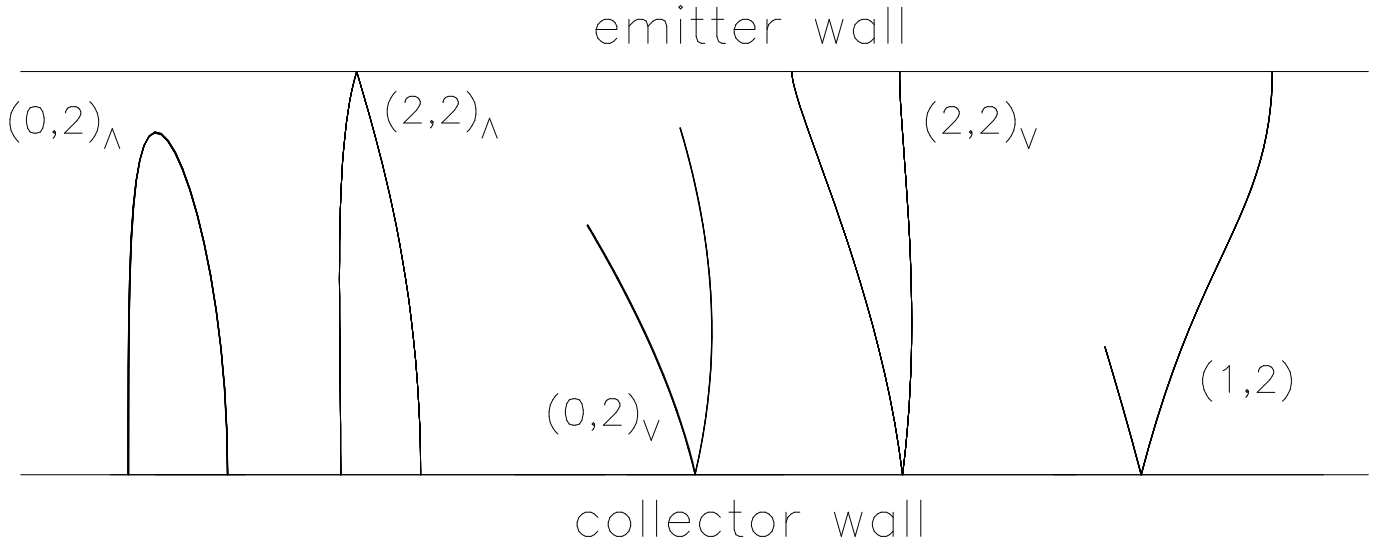


FIG. 7. Examples of the different types of period-2 orbits in  $y$ - $z$  projection. At higher magnetic fields similar orbits arise with one or more extra turns around the magnetic field direction.

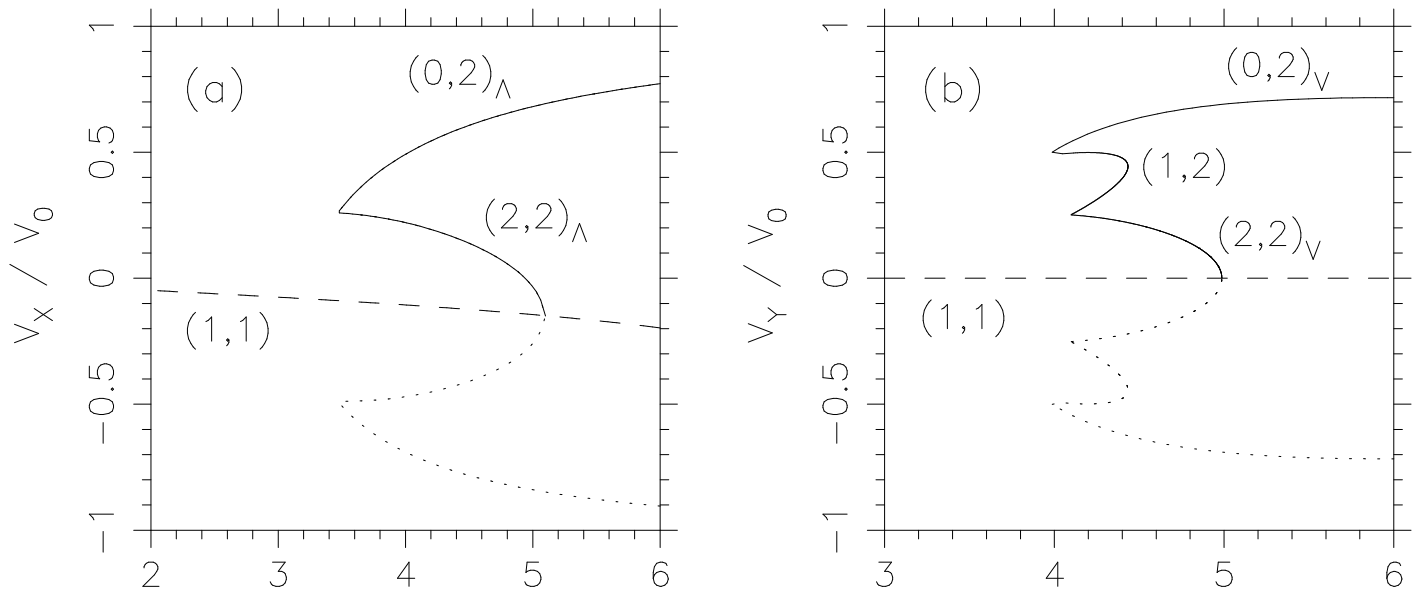


FIG. 8. The bifurcation diagrams of the period-2  $\Lambda$ -orbits (a) [ $\theta = 11^\circ$ ] and  $V$ -orbits (b) [ $\theta = 17^\circ$ ]. Each of the period-2 orbits is represented by its velocity [ $v_x$  for  $\Lambda$ -orbits and  $v_y$  for  $V$ -orbits] at the collisions with the collector barrier, with the velocity at the first collision shown by solid line, and the velocity at the second bounce shown by dotted line. The dashed line represents the period-1 orbit  $(1,1)$ .

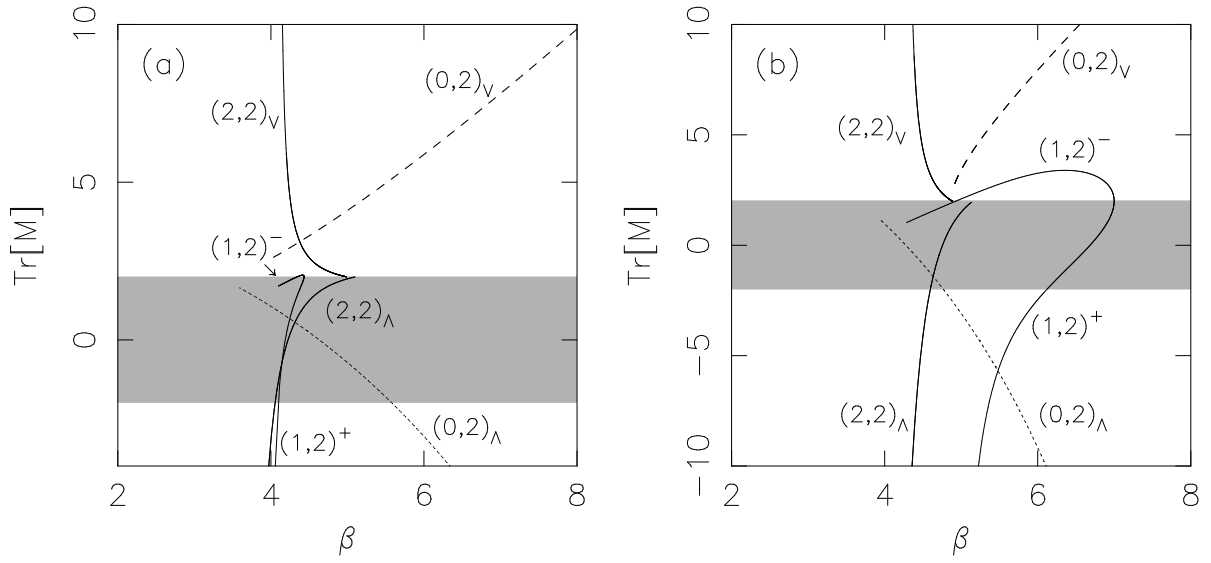


FIG. 9. The trace of the monodromy matrix for different period-2 orbits at (a)  $\theta = 17^\circ$  and (b)  $\theta = 28^\circ$ . All these period-two orbits appear in cusp bifurcation. One cusp bifurcation produces the  $\Lambda$ -orbits  $(0,2)_\Lambda$  and  $(2,2)_\Lambda$ , another cusp bifurcation generates the orbits  $(1,2)^-$  and  $(2,2)_V$ , and yet another cusp bifurcation produces  $(0,2)_V$  and  $(1,2)^+$ . Note the discontinuity of the trace of the monodromy matrix of the “more connected” partners  $(2,2)_\Lambda$ ,  $(2,2)_V$  and  $(1,2)^+$ . The single “metastable” orbit  $(1,2)^-$  leads to a strong scarring, it’s interval of existence substantially increases with the tilt angle.

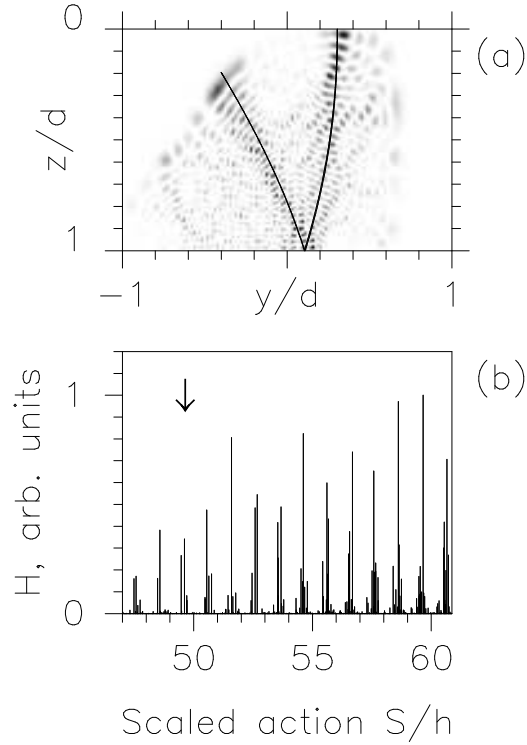


FIG. 10. A wavefunctions scarred by unstable  $(1, 2)^-$  orbit with  $y$ - $z$  projections of orbit superimposed (a), and the “Scar strength”  $H$  vs. the scaled action  $S(\varepsilon_n)/h$  of the  $(1, 2)^-$  orbit which scars the eigenstate of energy  $\varepsilon_n$ . The arrow indicates the value of  $\beta$  for the tangent bifurcation, which give birth to the periodic orbit. Note that when increasing action (or energy) the tangent bifurcation at higher  $\beta \sim 1/\sqrt{\varepsilon}$  occurs at the *lower* action side. The peaks of the scar strength below the tangent bifurcation are due to the “ghost effect”<sup>16,48</sup>. Scaled action below the bifurcation points is obtained by linear extrapolation of the (approximately linear) function  $S(\varepsilon)/h$ . “Scar strength”  $H$  is defined as the value of the Husimi function  $H(y^0, p_y^0) \equiv \int dy dp_y W_n(y, p_y) \exp(-(y - y^0)/l_B^2 - l_B^2(p_y - p_y^0)^2/\hbar)$  calculated for the normal derivative of the wavefunction ( $W_n(y, p_y) = \hbar^{-1} \int d\Delta y \partial_z \Psi(y - \Delta y/2, 0) \partial_z \Psi(y + \Delta y/2, 0) \exp(ip_y \Delta y/\hbar)$ ) at the location of the fixed point ( $y^0 \propto v_x, p_y^0 \propto v_y$ ) of the unstable periodic orbit.

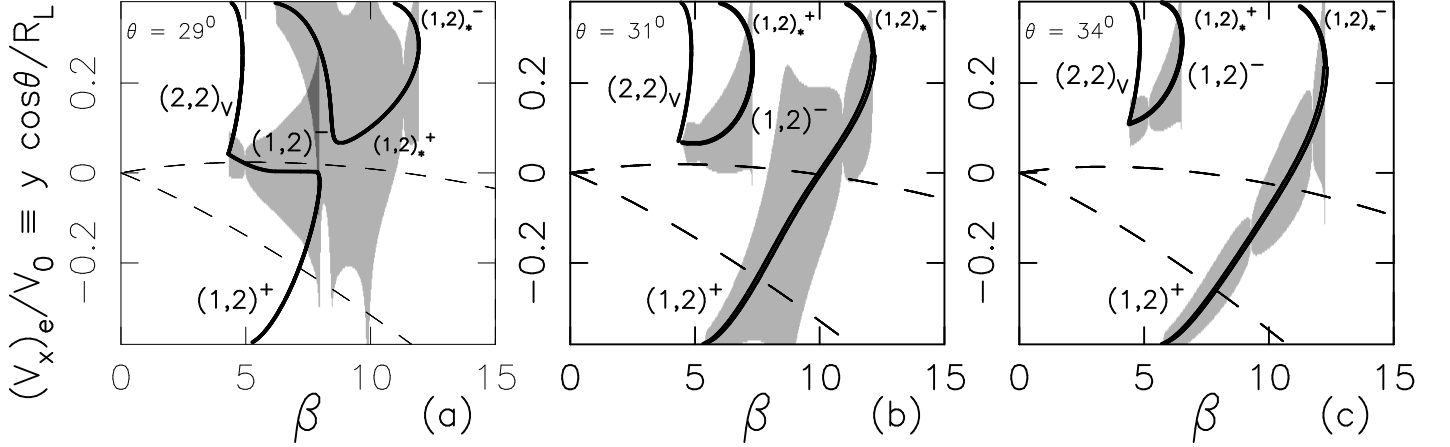


FIG. 11. Bifurcation diagrams for the four period-two orbits relevant to the peak-doubling in the interval  $\theta = 29^\circ - 34^\circ$  (see text). Thick lines indicate  $y$ -coordinate of the single collision with the emitter; these lines coincide at bifurcations.  $\theta = 29^\circ$  (a) indicates behavior before the exchange bifurcation;  $\theta = 31^\circ$  (b) and  $34^\circ$  (c) after. Shading represents the localization lengths  $l_\mu$  associated with the relevant orbits  $[(1, 2)^-$  and  $(1, 2)_*^+$  for (a), and  $(1, 2)^-$  and  $(1, 2)^+$  for (b),(c)]. Region between the dashed lines denotes semiclassical width of emitter state; overlap indicates a large contribution to the tunneling current.

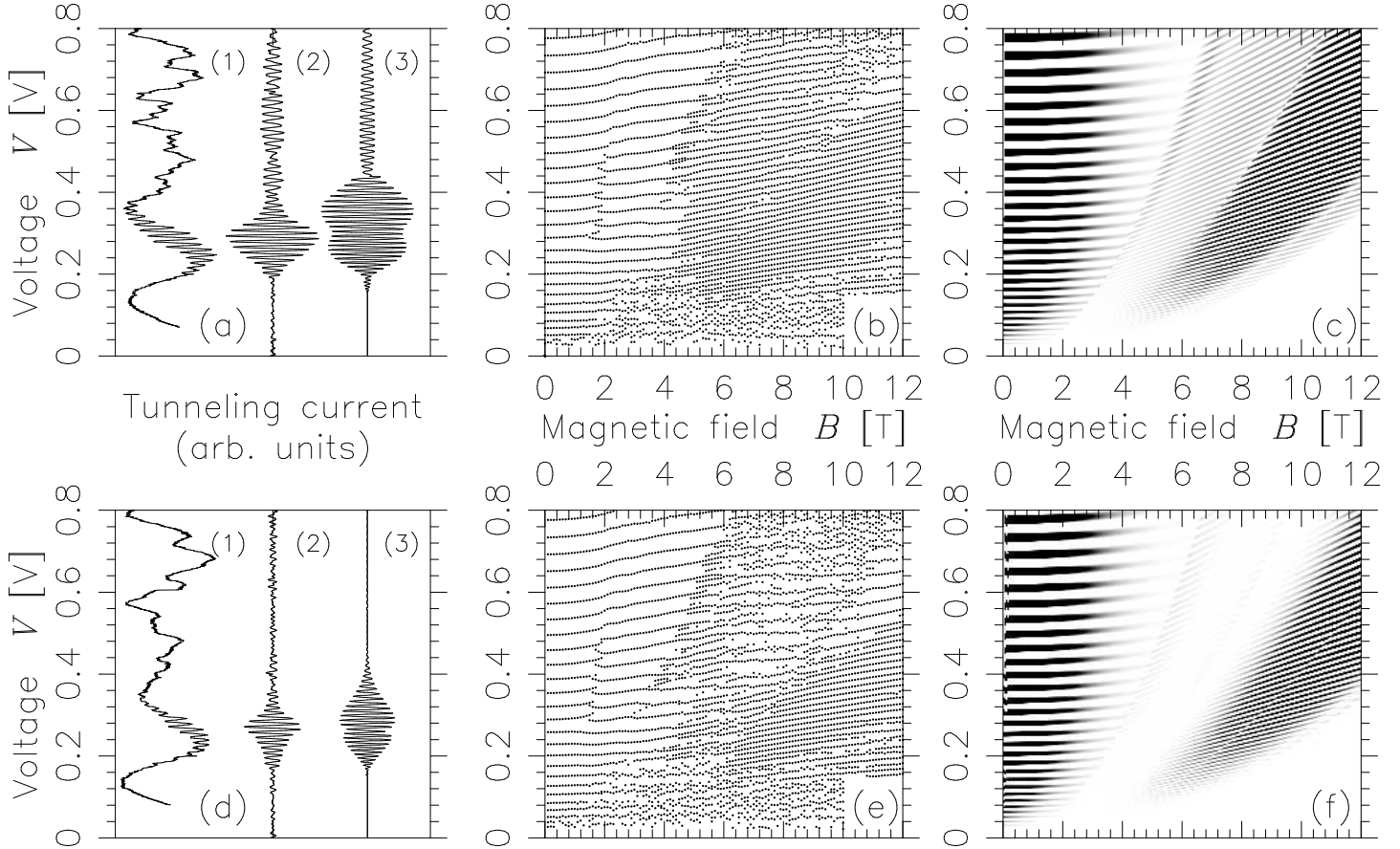


FIG. 12. Figs. (a),(d): resonant tunneling  $I - V$  traces for  $\theta = 31^\circ, \theta = 34^\circ$  at  $B = 8\text{T}$ . Trace (1) is raw experimental data, trace (2) is same data, filtered to retain only period-two oscillations, trace (3) is semiclassical prediction from Eq. (20). The modest discrepancies in the shape of the envelope of the amplitude of the oscillations are due to the inaccuracy of the quadratic semiclassical theory near the bifurcation which occurs around  $0.3\text{V}$  at  $8\text{T}$ . Figs. (b),(e): peak positions vs. voltage and magnetic field, determined from multiple sets of experimental  $I - V$  data at  $\theta = 31^\circ, 34^\circ$ . Figs. (c),(f): semiclassical  $I-V$  oscillations for same, note gray-scale indicates relative amplitudes, not just peak positions. Note disappearance of high voltage oscillations at  $\theta = 34^\circ$  due to movement of  $(1, 2)^-$  orbit away from accessibility after the exchange bifurcation (see Figs. 11b, 11c and text) [The Figure is reprinted from Ref.<sup>5</sup>].

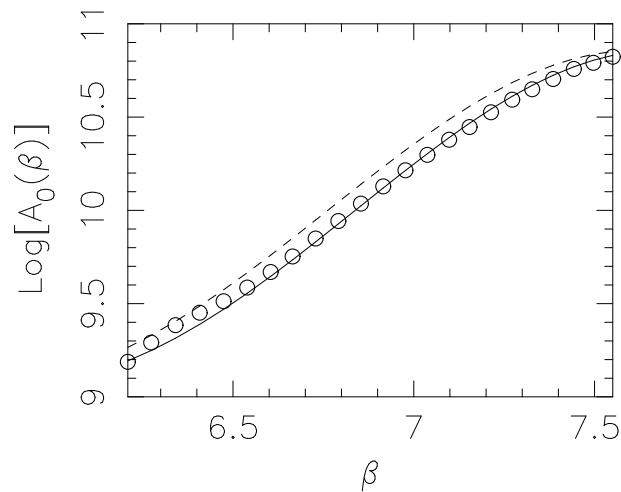




FIG. 13. The dependence of the amplitude of “ghost” oscillations on  $\beta$  for  $\theta = 11^\circ$ . The open circles represent the results of the exact calculation. The dashed line corresponds to the semiclassical formula (29). The solid line corresponds to the semiclassical calculation, which takes into account the transverse energy  $\kappa\hbar\omega_c$ , with  $\kappa = 0.55$ . This is in a good agreement with a simple estimate of  $\kappa \approx 0.42$  from the transverse energy of the *stable*  $(0, 1)^+$  orbit, which is soon to be born in the tangent bifurcation.

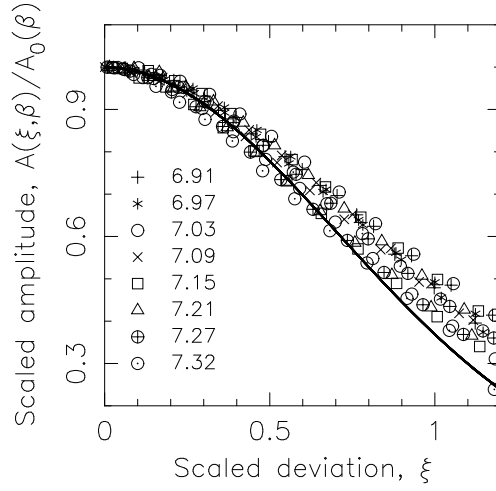


FIG. 14. The dependence of the scaled amplitude on the scaled deviation  $\xi$  from its maximum value. The solid line represents the functional form (31). Different symbols represent the results of the exact calculation for different  $\beta$ 's, with the corresponding values shown in the inset. Since the result (31) is based on the expansion near  $\xi = 0$ , the deviations from the semiclassical result increase for larger  $\xi$ .

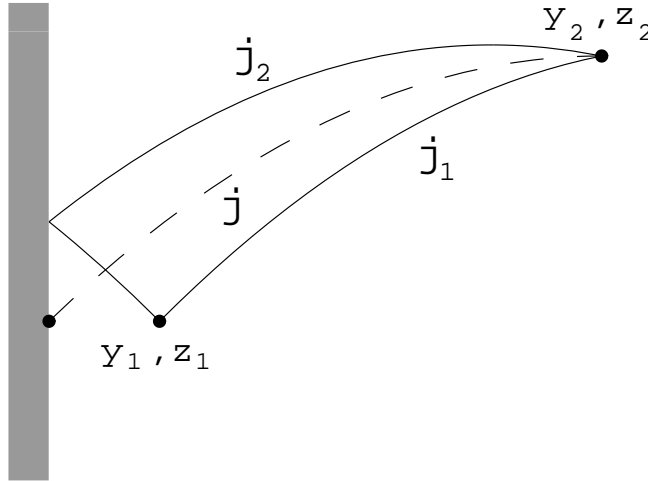


FIG. 15. The classical trajectories, which contribute to  $G(y_1, z_1; y_2, z_2)$  for  $z_1 \rightarrow +0$ .